

This chapter begins with a brief description of the qualitative character of turbulent flow. This is followed by the decomposition of a turbulent flow into a mean and fluctuating parts, and the derivation of the Reynolds-averaged Navier-Stokes (RANS) equations, the turbulent kinetic-energy equation, and the equation for the transport of the so-called Reynolds stress, which arises from the time averaging. These equations represent the foundation on which turbulence modelling is based. Reduced forms of the RANS equations for two-dimensional boundary-layer and Couette flows are then derived. The Law of the Wall is shown to result from dimensional considerations applied to plane Couette flow. Three separate zones are identified: the viscous sublayer, the fully-turbulent log-law region, and the buffer layer which separates the two. The Law of the Wake for the outer region of a turbulent boundary layer is then presented. A brief discussion follows concerned with the wide spectrum of length, time, and velocity scales, which are an important aspect of any turbulent flow. The log law is then applied to the analysis of turbulent flow through a smooth-walled pipe, followed by consideration of the effect of surface roughness. The calculation of pressure loss in piping systems is presented, largely based on empirical loss coefficients for such components as elbows, tee junctions, and area changes, together with the frictional pressure drop in long sections of pipe. Both the log-law and power-law velocity distributions are used as a basis for the analysis of a flat-plate turbulent boundary layer, and the results compared with empirical skin-friction formulae. The flow over a circular cylinder in crossflow is discussed based upon the experimentally based curve for the drag coefficient C_D versus Reynolds number, Re . Values of C_D are given for cylinders of various cross section in crossflow and also for a number of three-dimensional objects.

18.1 Transitional and turbulent flow

For any given **shear flow**¹⁶⁶, as the Reynolds number is progressively increased, some regions of the flowfield exhibit an unsteady (i.e. time-dependent) but still relatively orderly, essentially laminar, state, while other zones increasingly show irregular, chaotic, fluctuations in velocity. The latter is called **turbulent flow**, while the intermittent mix of quasi-laminar and turbulent flow is termed **transitional flow**. The **intermittency factor** γ at a fixed point in a flow is the fraction of time the flow there is turbulent, so that γ ranges from 0 to 1. As a consequence of

¹⁶⁶ Any flow in which viscous or turbulent shear stresses play a key role is termed a shear flow. Examples include duct flow, boundary-layer flow, free and wall jets, and wakes.

the velocity differences and overall scales involved, most flows of industrial interest fall into the turbulent-flow category.

It is generally accepted that any flow of a Newtonian fluid, whether laminar, transitional, or turbulent, obeys the **Navier-Stokes equations**. Although turbulent flow is inherently unsteady, a time average can be taken leading to a set of equations for the time-averaged motion. As we show in Section 18.2, these equations closely resemble the laminar-flow equations of Chapter 17 but include additional terms, the so-called **Reynolds stresses**, which arise as a consequence of correlations between the fluctuations in the three velocity components, u' , v' , and w' . Accounting for these correlations is the central problem in the analysis of time-averaged turbulent flows.

In principle the Navier-Stokes equations for the fluctuating motion can be converted to finite-difference, finite-volume, or finite-element form (a process called **discretisation**) and solved numerically, an approach known as **direct numerical simulation (DNS)**. In the case of a turbulent boundary layer, such a simulation has to account for all length scales, ranging from the Kolmogorov length scale¹⁶⁷ l_k to the boundary-layer thickness δ itself. Since a fluid volume of length L , width W , and thickness δ contains $WL\delta/l_k^3$ cells of side length l_k , this is the number of cells which would have to be considered in a complete simulation. With typical values $L = W = 1$ m, $\delta = 50$ mm, and $l_k = 50$ μ m, we find that this corresponds to 10^{15} (or 1000 trillion) cells, which exceeds the capacity of present-day computers and it is unlikely that DNS will be used for routine engineering calculations in the foreseeable future. Computing power, measured in flop/s, has increased exponentially over the last six decades, roughly according to $\text{flop/s} \approx e^{0.5\Delta y}$, where Δy is the number of years from 1938¹⁶⁸ at which we have set $\text{flop/s} = 1$. The fastest computer as of June 2015 is reported to have achieved close to 34 petaflops, i.e. 10^{15} flop/s.

18.2 Reynolds decomposition, Reynolds averaging, and Reynolds stresses

At any point within a turbulent flow, the three orthogonal components of the velocity, u , v , and w , together with the static pressure p , fluctuate apparently randomly with time. In general, it would be necessary to include the density in this list, but we shall limit consideration to constant-density flows. These fluctuations are subject to a number of constraints and so cannot be completely random: the continuity equation 15.7 for the flow of a constant-density fluid shows that u , v , and w are not independent, while p is related to u , v , and w through the Navier-Stokes equations 15.29 to 15.31.

Since DNS for practical engineering calculations is at best a prospect for the distant future, it is probable that for the foreseeable future the method of analysing turbulent flow, suggested by Osborne Reynolds in 1895, will be based upon separating all flow quantities into a mean (or time-averaged) part and a fluctuating (time-dependent) part, the latter having an average value

¹⁶⁷ The Kolmogorov length scale, together with other turbulence scales, is discussed in Section 18.4.

¹⁶⁸ The year 1938 is a consequence of extrapolating to zero a linear fit to a graph of computing power (flop/s) versus calendar year on log-linear coordinates.

of zero. This is known as **Reynolds decomposition**. If we take the x -component of velocity u , to illustrate this idea, we have

$$u = \bar{u} + u' \quad (18.1)$$

where \bar{u} is the time average¹⁶⁹ of the fluctuating velocity u and u' is the fluctuating part. The time average is defined by

$$\bar{u} = \frac{1}{T} \int_0^T u \, dt \quad (18.2)$$

where the time interval T over which the average is taken is long compared with the fluctuating time scale. The overbar¹⁷⁰ here and elsewhere signifies a time average. Substitution of $u = \bar{u} + u'$ into equation (18.2) leads immediately to $\bar{u'} = 0$. As we shall see shortly, when we apply this type of averaging process to the Navier-Stokes equations, non-zero terms like $\overline{u'^2}$ and $\overline{u'v'}$ arise.

According to equation (15.7), for an incompressible flow the continuity equation is

$$\frac{\partial u}{\partial x} + \frac{\partial v}{\partial y} + \frac{\partial w}{\partial z} = 0 \quad (18.3)$$

which we can now write as

$$\frac{\partial (\bar{u} + u')}{\partial x} + \frac{\partial (\bar{v} + v')}{\partial y} + \frac{\partial (\bar{w} + w')}{\partial z} = 0. \quad (18.4)$$

If we take the time average of equation (18.4), the three fluctuating terms average to zero and we have

$$\frac{\partial \bar{u}}{\partial x} + \frac{\partial \bar{v}}{\partial y} + \frac{\partial \bar{w}}{\partial z} = 0. \quad (18.5)$$

If we subtract equation (18.5) from equation (18.4) we find

$$\frac{\partial u'}{\partial x} + \frac{\partial v'}{\partial y} + \frac{\partial w'}{\partial z} = 0 \quad (18.6)$$

and we see that the mean and fluctuating parts of the instantaneous velocity components separately satisfy an equation of continuity.

From Subsection 15.1.6 the three components of the Navier-Stokes equations for the flow of a constant- and uniform-property fluid in the absence of body forces are:

x -component

$$\rho \frac{Du}{Dt} = \rho \left[\frac{\partial u}{\partial t} + \frac{\partial u^2}{\partial x} + \frac{\partial (uv)}{\partial y} + \frac{\partial (uw)}{\partial z} \right] = -\frac{\partial p}{\partial x} + \mu \left(\frac{\partial^2 u}{\partial x^2} + \frac{\partial^2 u}{\partial y^2} + \frac{\partial^2 u}{\partial z^2} \right) \quad (18.7)$$

¹⁶⁹ To avoid confusion, we shall assume that \bar{u} is independent of time. However, just as we can have an unsteady laminar flow, we can also have a turbulent flow for which \bar{u} varies with time at a frequency much lower than is typical of the turbulent fluctuations.

¹⁷⁰ Angle brackets are sometimes used instead of an overbar to denote a time average, i.e. $u = \bar{u}$.

y-component

$$\rho \frac{Dv}{Dt} = \rho \left[\frac{\partial v}{\partial t} + \frac{\partial(vu)}{\partial x} + \frac{\partial v^2}{\partial y} + \frac{\partial(vw)}{\partial z} \right] = -\frac{\partial p}{\partial y} + \mu \left(\frac{\partial^2 v}{\partial x^2} + \frac{\partial^2 v}{\partial y^2} + \frac{\partial^2 v}{\partial z^2} \right) \quad (18.8)$$

z-component

$$\rho \frac{Dw}{Dt} = \rho \left[\frac{\partial w}{\partial t} + \frac{\partial(wu)}{\partial x} + \frac{\partial(wv)}{\partial y} + \frac{\partial w^2}{\partial z} \right] = -\frac{\partial p}{\partial z} + \mu \left(\frac{\partial^2 w}{\partial x^2} + \frac{\partial^2 w}{\partial y^2} + \frac{\partial^2 w}{\partial z^2} \right). \quad (18.9)$$

In each of these equations we have replaced terms like $v\partial u/\partial y$ by $\partial(uv)/\partial y - u\partial v/\partial y$ and used the continuity equation to eliminate $\partial v/\partial y$ ¹⁷¹.

If we now take the time averages of these three equations we have, for a flow which is steady on average

$$\rho \left[\frac{\partial \bar{u}^2}{\partial x} + \frac{\partial(\bar{u}\bar{v})}{\partial y} + \frac{\partial(\bar{u}\bar{w})}{\partial z} \right] = -\frac{\partial \bar{p}}{\partial x} + \mu \left(\frac{\partial^2 \bar{u}}{\partial x^2} + \frac{\partial^2 \bar{u}}{\partial y^2} + \frac{\partial^2 \bar{u}}{\partial z^2} \right) \quad (18.10)$$

$$\rho \left[\frac{\partial(\bar{v}\bar{u})}{\partial x} + \frac{\partial \bar{v}^2}{\partial y} + \frac{\partial(\bar{v}\bar{w})}{\partial z} \right] = -\frac{\partial \bar{p}}{\partial y} + \mu \left(\frac{\partial^2 \bar{v}}{\partial x^2} + \frac{\partial^2 \bar{v}}{\partial y^2} + \frac{\partial^2 \bar{v}}{\partial z^2} \right) \quad (18.11)$$

$$\rho \left[\frac{\partial(\bar{w}\bar{u})}{\partial x} + \frac{\partial(\bar{w}\bar{v})}{\partial y} + \frac{\partial \bar{w}^2}{\partial z} \right] = -\frac{\partial \bar{p}}{\partial z} + \mu \left(\frac{\partial^2 \bar{w}}{\partial x^2} + \frac{\partial^2 \bar{w}}{\partial y^2} + \frac{\partial^2 \bar{w}}{\partial z^2} \right). \quad (18.12)$$

It should now be clear that the difference between the Navier-Stokes equations for a steady laminar flow and for a time-mean-steady turbulent flow arises from the non-linear advective terms on the left-hand side of each of the last three equations.

If we now introduce $u = \bar{u} + u'$, $v = \bar{v} + v'$, and $w = \bar{w} + w'$, we have

$$\bar{u}^2 = \bar{u}^2 + \overline{u'u'}, \quad \bar{u}\bar{v} = \bar{u}\bar{v} + \overline{u'v'}, \quad \text{and} \quad \bar{u}\bar{w} = \bar{u}\bar{w} + \overline{u'w'}, \quad \text{etc.} \quad (18.13)$$

In arriving at these identities we have made use of the fact that $\overline{u'u} = \overline{u'u} = 0$, $\overline{v'v} = \overline{v'v} = 0$, etc.

Equation (18.10) may now be written as

$$\rho \left[\frac{\partial}{\partial x} (\bar{u}^2 + \overline{u'u'}) + \frac{\partial}{\partial y} (\bar{u}\bar{v} + \overline{u'v'}) + \frac{\partial}{\partial z} (\bar{u}\bar{w} + \overline{u'w'}) \right] = -\frac{\partial \bar{p}}{\partial x} + \mu \left(\frac{\partial^2 \bar{u}}{\partial x^2} + \frac{\partial^2 \bar{u}}{\partial y^2} + \frac{\partial^2 \bar{u}}{\partial z^2} \right)$$

which simplifies to

$$\begin{aligned} \rho \left(\bar{u} \frac{\partial \bar{u}}{\partial x} + \bar{v} \frac{\partial \bar{u}}{\partial y} + \bar{w} \frac{\partial \bar{u}}{\partial z} \right) &= -\frac{\partial \bar{p}}{\partial x} + \frac{\partial}{\partial x} \left(\mu \frac{\partial \bar{u}}{\partial x} - [\rho \overline{u'u'}] \right) + \frac{\partial}{\partial y} \left(\mu \frac{\partial \bar{u}}{\partial y} - [\rho \overline{u'v'}] \right) \\ &\quad + \frac{\partial}{\partial z} \left(\mu \frac{\partial \bar{u}}{\partial z} - [\rho \overline{u'w'}] \right) \end{aligned} \quad (18.14)$$

equation (18.11) may be written as

$$\rho \left[\frac{\partial}{\partial x} (\bar{v}\bar{u} + \overline{v'u'}) + \frac{\partial}{\partial y} (\bar{v}^2 + \overline{v'v'}) + \frac{\partial}{\partial z} (\bar{v}\bar{w} + \overline{v'w'}) \right] = -\frac{\partial \bar{p}}{\partial y} + \mu \left(\frac{\partial^2 \bar{v}}{\partial x^2} + \frac{\partial^2 \bar{v}}{\partial y^2} + \frac{\partial^2 \bar{v}}{\partial z^2} \right)$$

¹⁷¹ This part of the analysis is the subject of Self-assessment problem 18.1.

which simplifies to

$$\begin{aligned} \rho \left(\bar{u} \frac{\partial \bar{v}}{\partial x} + \bar{v} \frac{\partial \bar{v}}{\partial y} + \bar{w} \frac{\partial \bar{v}}{\partial z} \right) = & - \frac{\partial \bar{p}}{\partial y} + \frac{\partial}{\partial x} \left(\mu \frac{\partial \bar{v}}{\partial x} - [\rho \bar{v}' u'] \right) + \frac{\partial}{\partial y} \left(\mu \frac{\partial \bar{v}}{\partial y} - [\rho \bar{v}' v'] \right) \\ & + \frac{\partial}{\partial z} \left(\mu \frac{\partial \bar{v}}{\partial z} - [\rho \bar{v}' w'] \right) \end{aligned} \quad (18.15)$$

and equation (18.12) may be written as

$$\rho \left[\frac{\partial}{\partial x} (\bar{w} \bar{u} + \overline{w' u'}) + \frac{\partial}{\partial y} (\bar{w} \bar{v} + \overline{w' v'}) + \frac{\partial}{\partial z} (\bar{w}^2 + \overline{w' w'}) \right] = - \frac{\partial \bar{p}}{\partial z} + \mu \left(\frac{\partial^2 \bar{w}}{\partial x^2} + \frac{\partial^2 \bar{w}}{\partial y^2} + \frac{\partial^2 \bar{w}}{\partial z^2} \right)$$

which simplifies to

$$\begin{aligned} \rho \left(\bar{u} \frac{\partial \bar{w}}{\partial x} + \bar{v} \frac{\partial \bar{w}}{\partial y} + \bar{w} \frac{\partial \bar{w}}{\partial z} \right) = & - \frac{\partial \bar{p}}{\partial z} + \frac{\partial}{\partial x} \left(\mu \frac{\partial \bar{w}}{\partial x} - [\rho \bar{w}' u'] \right) + \frac{\partial}{\partial y} \left(\mu \frac{\partial \bar{w}}{\partial y} - [\rho \bar{w}' v'] \right) \\ & + \frac{\partial}{\partial z} \left(\mu \frac{\partial \bar{w}}{\partial z} - [\rho \bar{w}' w'] \right). \end{aligned} \quad (18.16)$$

Equations (18.14), (18.15), and (18.16) are known as the **Reynolds-averaged Navier-Stokes** (or **RANS**) **equations**. It is the terms in square brackets in these equations which distinguish them from their laminar-flow counterparts. In fact, if the velocity fluctuations are zero, the RANS equations reduce to those for steady, constant-property, laminar flow. From now on we shall write $\overline{u' u'}$, $\overline{v' v'}$, and $\overline{w' w'}$ as $\overline{u'^2}$, $\overline{v'^2}$, and $\overline{w'^2}$, respectively. These additional terms, usually shifted to appear on the right-hand sides of the time-averaged Navier-Stokes equations, by comparison with the viscous normal and shear stresses, may be interpreted physically as stresses: $\rho \overline{u'^2}$, $\rho \overline{v'^2}$, and $\rho \overline{w'^2}$ as pressure-like normal stresses, and $\rho \overline{u' v'}$, $\rho \overline{v' w'}$, and $\rho \overline{w' u'}$ as shear stresses. The six stresses are known as the **Reynolds stresses**¹⁷² or **apparent stresses**. Each of the shear stresses arises from the correlation of two orthogonal components of the velocity fluctuation at a given point, a non-zero value of the correlation indicating that the two components are not independent. If the correlation is negative, then the two components are opposite in sign over most of the averaging period.

18.3 Turbulent-kinetic-energy equation and Reynolds-stress equation

At any point in a turbulent flow, half the sum of the three normal stresses represents the **specific turbulent kinetic energy**¹⁷³ \bar{k} , of the fluctuating velocity components

$$\bar{k} = \frac{1}{2} \left(\overline{u'^2} + \overline{v'^2} + \overline{w'^2} \right). \quad (18.17)$$

Since it is often the case that there is a principal flow direction, for example the x -direction, it is common to take the value of $\overline{u'^2}$ as a measure of the turbulence intensity. Other measures

¹⁷² The quantities $\overline{u'^2}$, $\overline{v'^2}$, $\overline{w'^2}$, $\overline{u' v'}$, $\overline{v' w'}$, and $\overline{w' u'}$ are also often referred to as the Reynolds stresses but, in the absence of the density ρ , the term **kinematic Reynolds stresses** is more appropriate.

¹⁷³ The specific turbulent kinetic energy is the turbulent kinetic energy per unit mass.

in use include $\sqrt{u'^2}/\bar{u}$, $\sqrt{u'^2}/U_\infty$, \sqrt{k}/\bar{u} , and \sqrt{k}/U_∞ . The normalising velocity, \bar{u} or U_∞ , is measured at the same location as u' .

In addition to the RANS equations, further exact equations can be derived from the Navier-Stokes equations. For example, for a steady, two-dimensional, constant-property, turbulent boundary layer, neglecting viscous terms other than the dissipation, we have the **turbulent-kinetic-energy equation**

$$\underbrace{\bar{u} \frac{\partial \bar{k}}{\partial x}}_{\text{I}} + \underbrace{\bar{v} \frac{\partial \bar{k}}{\partial y}}_{\text{II}} = - \underbrace{\frac{\partial}{\partial y} \left[\bar{v}' \left(\frac{1}{2} k + \frac{p'}{\rho} \right) \right]}_{\text{III}} + \underbrace{\left(\bar{v} \frac{\partial \bar{u}}{\partial y} - \overline{u'v'} \right) \frac{\partial \bar{u}}{\partial y}}_{\text{IV}} - \epsilon \quad (18.18)$$

where ϵ is the average **turbulent-kinetic-energy dissipation rate**¹⁷⁴ given by

$$\epsilon = \nu \left[2 \left(\frac{\partial u'}{\partial x} \right)^2 + 2 \left(\frac{\partial v'}{\partial y} \right)^2 + 2 \left(\frac{\partial w'}{\partial z} \right)^2 + \left(\frac{\partial u'}{\partial y} + \frac{\partial v'}{\partial x} \right)^2 + \left(\frac{\partial u'}{\partial z} + \frac{\partial w'}{\partial x} \right)^2 + \left(\frac{\partial v'}{\partial z} + \frac{\partial w'}{\partial y} \right)^2 \right]. \quad (18.19)$$

The combination $\rho \left(\bar{v} \frac{\partial \bar{u}}{\partial y} - \overline{u'v'} \right)$ is the combined viscous-plus-turbulent time-average shear stress $\bar{\tau}$ and, apart from the region close to a solid boundary, it is usually the case that $-\overline{u'v'} \gg \bar{v} \frac{\partial \bar{u}}{\partial y}$. In addition to ϵ , the turbulent kinetic-energy equation has introduced two further turbulence correlations: $\overline{v'k}$ and $\overline{v'p'}$.

The terms in equation (18.18) can be interpreted as follows

- I. Transport of k through advection by the mean flow
- II. Transport of k by velocity fluctuations (turbulent diffusion)
- III. Transport of k by pressure fluctuations
- IV. Rate of production of k by interaction of the shear stress and the mean-velocity gradient

It should be noted that dissipation of kinetic energy also occurs due to the velocity gradients of the time-mean motion (so-called **direct dissipation**).

Another equation commonly considered in two-dimensional turbulent boundary-layer analysis is the **Reynolds-stress equation**

$$\begin{aligned} \bar{u} \frac{\partial \left(-\overline{u'v'} \right)}{\partial x} + \bar{v} \frac{\partial \left(-\overline{u'v'} \right)}{\partial y} &= \bar{v}^2 \frac{\partial \bar{u}}{\partial y} - \frac{p'}{\rho} \left(\frac{\partial u'}{\partial y} + \frac{\partial v'}{\partial x} \right) + \frac{\partial}{\partial y} \left(\overline{u'v'^2} + \frac{p'u'}{\rho} \right) \\ &\quad + \nu \frac{\partial^2 \left(-\overline{u'v'} \right)}{\partial y^2} + 2\nu \frac{\partial u'}{\partial y} \frac{\partial v'}{\partial x} \end{aligned} \quad (18.20)$$

which has again introduced further terms.

The turbulent kinetic-energy equation, the Reynolds-stress equation, and other equations derived from or based on the RANS equations are the foundations for the methodology termed turbulence modelling, which we discuss briefly in Section 18.5.

¹⁷⁴ The symbol ϵ represents the lower-case Greek letter epsilon. Epsilon is also represented by ε , which we use for surface-roughness height (see Section 18.9).

18.4 Turbulence scales

So far we have made little mention of the structure of a turbulent flow. It is observed experimentally that clumps (or packets) of fluid particles, called **eddies**, form, interact, break up, and reform throughout a turbulent flow. The length scale (i.e. size) of these eddies varies from the overall scale of the flow down to a **microscale**, much larger than the **molecular mean free path**, so that the **continuum hypothesis** still applies (already implied in assuming that the Navier-Stokes equations apply), where viscosity dominates and turbulent kinetic energy is dissipated into heat. Most of the kinetic energy of a turbulent flow is contained in the **integral length scales**, which are the largest scales in an energy spectrum, i.e. the distribution of kinetic energy according to length scale or frequency. The largest scales correspond to the lowest frequency, and vice versa. The kinetic energy in a turbulent flow passes progressively from the largest energy-bearing eddies to the smallest dissipative eddies in what is termed the **energy cascade**. It should be evident that, because there are fluctuations in velocity and a wide distribution of length scales, **mixing** within a turbulent flow is much stronger than in a laminar flow. The practical consequence is enhanced surface shear stress and, where a surface is heated or cooled, higher rates of heat transfer than in a laminar flow.

The smallest length scale at which turbulence can exist in a flow is the **Kolmogorov length scale** l_K , defined in terms of the kinematic viscosity of the fluid ν and the rate of dissipation of turbulent kinetic energy per unit mass ϵ

$$l_K = \left(\frac{\nu^3}{\epsilon} \right)^{1/4}. \quad (18.21)$$

This combination of ν and ϵ is arrived at on dimensional grounds since $[\nu] = L^2/T$, and $[\epsilon] = L^2/T^3$. The **Kolmogorov time** and **velocity scales**, τ_K and v_K , are similarly defined

$$\tau_K = \left(\frac{\nu}{\epsilon} \right)^{1/2} \quad (18.22)$$

and

$$v_K = (\nu\epsilon)^{1/4}. \quad (18.23)$$

An inevitable consequence of these definitions is that the Reynolds number $v_K l_K / \nu = 1$, indicating that the small-scale motion is quite viscous. In numerical simulations of turbulent flows, the smallest scale that has to be resolved is usually taken to be of the same order of magnitude as the Kolmogorov length scale.

At any point in a turbulent flow, fluctuations in velocity and pressure contain energy across a wide range of frequencies f . According to equation (18.17), the turbulent kinetic energy per unit mass is k

$$\bar{k} = \frac{1}{2} \left(\overline{u'^2} + \overline{v'^2} + \overline{w'^2} \right) \quad (18.17)$$

and, if the kinetic energy in the frequency range f to $f + \delta f$ is $E(f)$, then

$$\bar{k} = \int_0^\infty E(f) df. \quad (18.24)$$

Rather than frequency, it is usual here to introduce the idea of a **wavenumber** κ , where

$$\kappa = \frac{2\pi f}{v} = \frac{2\pi}{\lambda} \quad (18.25)$$

and $\lambda = v/f$ is the wavelength, v being the instantaneous velocity at the point of measurement. Equation (18.24) is then written as

$$\bar{k} = \int_0^\infty E(\kappa) d\kappa \quad (18.26)$$

and the quantity $E(k)$ is called the **energy spectral density**, or **energy spectrum function**.

The so-called **inertial subrange** corresponds with the non-dissipative **Taylor microscales**, which are intermediate between the largest and smallest scales. Within the inertial subrange Kolmogorov argued that a range of scales exists within which $E(\kappa)$ is dependent upon the dissipation rate ϵ and wavenumber κ but independent of viscosity so that

$$E(\kappa) = F(\epsilon, \kappa). \quad (18.27)$$

It follows from dimensional analysis that

$$E = C_K \epsilon^{2/3} \kappa^{-5/3} \quad (18.28)$$

where C_K is the **Kolmogorov constant**. The inertial subrange covers the wavenumber range $1/l \ll \kappa \ll 1/l_K$, where l is a measure of the largest scale, such as the **integral length scale**.

If it is assumed, as is reasonable, that the turbulence dissipation rate ϵ is determined by the specific turbulent kinetic energy k and the integral length scale l , then dimensional analysis leads to

$$\epsilon \sim \frac{k^{3/2}}{l}. \quad (18.29)$$

For Couette flow, the convective terms on the left-hand side of the **turbulent kinetic-energy equation** (18.18) are zero, and \bar{u} is independent of x , so we have

$$-\frac{\partial}{\partial y} \left[v' \left(\frac{1}{2} k + \frac{p'}{\rho} \right) \right] + \left(v \frac{\partial \bar{u}}{\partial y} - \overline{u'v'} \right) \frac{d\bar{u}}{dy} - \epsilon = 0. \quad (18.30)$$

It can be shown that the term involving $\overline{v'k}$ and $\overline{v'p'}$ is negligible compared with the production and dissipation terms, so that equation (18.30) reduces to

$$\epsilon = -\overline{u'v'} \frac{d\bar{u}}{dy} \quad (18.31)$$

where we have neglected the viscous shear stress compared with the Reynolds shear stress.

In Subsection 18.7.2 we show that, for the near-wall region, if $-\rho \overline{u'v'} = \tau_s$, then

$$\frac{\gamma}{u_\tau} \frac{d\bar{u}}{dy} = \frac{1}{k} \quad (18.50)$$

so that from equation (18.31)

$$\epsilon = \frac{u_\tau^3}{\kappa y} \quad (18.32)$$

and we have a good estimate for ϵ in the log-law region.

From the definitions of the Kolmogorov scales (equations (18.21) to (18.23)) we then have

$$\frac{u_\tau l_k}{\nu} = (\kappa y^+)^{1/4} \quad (18.33)$$

$$\frac{u_\tau^2 \tau_K}{\nu} = (\kappa y^+)^{1/2} \quad (18.34)$$

and

$$\frac{v_K}{u_\tau} = \frac{1}{(\kappa y^+)^{1/4}}. \quad (18.35)$$

In Illustrative Example 18.2 we calculate values for the Kolmogorov scales for a specified pipe flow.

18.5 Turbulence modelling

Unfortunately, it is unlikely that physically exact equations will ever be established which take into account the entire range of length and time scales which we have just identified and which link the six Reynolds stresses, and correlations such as $\overline{p'u'}$, $\overline{u'v'^2}$, etc., to \overline{u} , \overline{v} , \overline{w} , \overline{p} , and their spatial gradients. Apart from research into DNS and the closely related **large-eddy simulation (LES)**, which avoids the need to establish such links, research hitherto has concentrated on a semi-empirical methodology in which the physics of turbulent flow is approximated by partial differential equations for the specific turbulent kinetic energy k , the rate of turbulent dissipation ϵ , the Reynolds stresses $\overline{u'v'}$, $\overline{u'^2}$, $\overline{v'^2}$, etc., and various length scales with approximations for the correlations between u' , v' , w' , p' , and their gradients. Devising these approximations has become known as **turbulence modelling**.

For the foreseeable future, DNS and LES are likely to remain research topics providing results used to guide the development of, and against which to test the predictions of, turbulence modelling, particularly where experimental data are unavailable. Depending upon the complexity involved and level of accuracy required, engineering applications will rely upon software based upon empirical correlations and turbulence modelling of varying levels of sophistication.

Probably the earliest example of turbulence modelling was Prandtl's **mixing-length hypothesis** based upon the idea that the large-scale random movements of fluid elements in turbulent motion are analogous to the small-scale random motion of molecules in a gas (kinetic theory). From this beginning, with time the following hierarchy of turbulence models has evolved

- zero equation model, such as the mixing-length or eddy-viscosity model
- two-equation model, in which time-averaged equations are solved for the specific turbulent-kinetic energy k and the turbulent-kinetic-energy dissipation rate ϵ
- Reynolds-stress equation model
- algebraic-stress model

A detailed presentation and discussion of turbulence modelling is beyond the scope of this text and from the foregoing the impression could be gained that little progress has been made

in devising relatively simple ways to analyse turbulent flows of practical interest. In fact much of what was learned throughout the 20th century, based upon simplifications, dimensional analysis, empiricism, and integral methods, forms the basis of current engineering practice and to a large extent is incorporated into turbulence modelling. Some of the ideas involved are discussed in the remainder of this chapter.

18.6 Two-dimensional turbulent boundary layers and Couette flow

Although velocity fluctuations in a turbulent flow always occur in the three orthogonal directions, there are many practical situations, just as for laminar flow, where there is no variation of time-averaged quantities in the third direction (usually taken as the z -direction). If in addition we introduce the boundary-layer approximations outlined in Chapter 17, the counterpart to equation (17.4) for a turbulent boundary layer is

$$\bar{u} \frac{\partial \bar{u}}{\partial x} + \bar{v} \frac{\partial \bar{u}}{\partial y} = -\frac{1}{\rho} \frac{dp}{dx} + \frac{1}{\rho} \frac{\partial}{\partial y} \left(\mu \frac{\partial \bar{u}}{\partial y} - \rho \overline{u'v'} \right). \quad (18.36)$$

Even though the Reynolds shear stress $\rho \overline{u'v'}$ is the only term remaining from the Reynolds decomposition and time averaging, except in the near-vicinity of a wall, it is usually several orders of magnitude greater than the viscous shear stress, $\mu \partial \bar{u} / \partial y$, and so has to be accounted for. Just as for laminar flow, we can consider fully-developed turbulent flow through a cylindrical channel, for which equation (18.36) reduces to

$$0 = -\frac{1}{\rho} \frac{dp}{dx} + \frac{1}{\rho} \frac{\partial}{\partial y} \left(\mu \frac{d\bar{u}}{dy} - \rho \overline{u'v'} \right). \quad (18.37)$$

A further simplification occurs for **Couette flow** which, as we saw in Section 16.4, is the fully-developed, shear-driven flow between two parallel surfaces where one is moving tangentially with respect to the other. Within such an idealised flow the shear stress is constant (giving rise to the term **constant-stress layer**) so that, if the flow is turbulent, the mean (i.e. time-averaged) shear stress $\bar{\tau}$ is given by

$$\bar{\tau} = \mu \frac{d\bar{u}}{dy} - \rho \overline{u'v'} = \text{constant} = \bar{\tau}_S \quad (18.38)$$

where $\bar{\tau}_S$ is the mean wall shear stress and y is the distance from the stationary surface.

The boundary conditions for equations (18.36), (18.37), and (18.38) are the same as those for laminar flow.

18.7 Plane turbulent Couette flow and the Law of the Wall

As we have just seen, for plane turbulent Couette flow the RANS equations reduce to

$$\bar{\tau} = \mu \frac{d\bar{u}}{dy} - \rho \overline{u'v'} = \text{constant} = \bar{\tau}_S. \quad (18.39)$$

Equation (18.39) cannot simply be integrated to give the mean-velocity profile $\bar{u}(y)$ because the dependence of the Reynolds shear stress $-\overline{u'v'}$ on other flow properties is unknown.

We shall return to equation (18.39) shortly but for the time being we introduce the assumption that \bar{u} depends upon y , $\bar{\tau}_s$, and the fluid properties ρ and μ , i.e.

$$\bar{u} = f(y, \bar{\tau}_s, \rho, \mu), \quad (18.40)$$

an assumption which can reasonably be applied to the near-wall region of any turbulent shear flow over a smooth surface, i.e. to boundary layers and channel flows. Dimensional analysis leads to

$$\frac{\bar{u}}{u_\tau} = f\left(\frac{u_\tau y}{\nu}\right) \quad (18.41)$$

where $u_\tau = \sqrt{\bar{\tau}_s/\rho}$ has the units of velocity and is termed the **friction velocity** (or **wall-friction velocity**)¹⁷⁵. Equation (18.41), first postulated by Prandtl, is known as the **Law of the Wall**, or **universal velocity distribution**, and written as

$$u^+ = f(y^+) \quad (18.42)$$

where

$$u^+ \equiv \frac{\bar{u}}{u_\tau} \text{ and } y^+ \equiv \frac{u_\tau y}{\nu} \quad (18.43)$$

are the so-called **wall variables**¹⁷⁶. It is seen that y^+ can be regarded as a turbulence Reynolds number and that ν/u_τ is a **viscous length scale**. The Law of the Wall is usually regarded as comprising three parts: a **viscous sublayer**, a **buffer layer**, and a **fully-turbulent region**.

18.7.1 Viscous sublayer

From the boundary conditions at a solid surface it must be that $u' = 0$ (the no-slip condition) and $v' = 0$ (impermeable surface) so that in the immediate vicinity of a solid surface both u' and v' decrease and $\mu d\bar{u}/dy \gg \rho \overline{u'v'}$. Equation (18.39) thus reduces to

$$\frac{d\bar{u}}{dy} = \frac{\bar{\tau}_s}{\mu} \quad (18.44)$$

which integrates to give

$$\bar{u} = \frac{\bar{\tau}_s y}{\mu} \quad (18.45)$$

or, in wall variables,

$$u^+ = y^+. \quad (18.46)$$

The region where equation (18.46) is valid is termed the **viscous** (or **linear**) **sublayer**¹⁷⁷ and taken to have a thickness δ_{SUB} given by

¹⁷⁵ The symbol u^* is also used to represent the friction velocity and spoken as 'ustar'.

¹⁷⁶ u^+ and y^+ are spoken as 'uplus' and 'yplus', respectively.

¹⁷⁷ Although the turbulence intensity is small, the flow within the viscous sublayer is not purely laminar, and the term **laminar sublayer** is to be avoided.

$$\frac{u_\tau \delta_{SUB}}{\nu} = \delta_{SUB}^+ = 5. \quad (18.47)$$

18.7.2 Fully-turbulent layer and the log law

Beyond the viscous sublayer, $y^+ > 30$, say, it is argued that direct viscous effects on the turbulent structure and the influence of viscosity on the mean flow is negligible so that the mean-velocity gradient is dependent only upon y , ρ , and $\bar{\tau}_s$, i.e.

$$\frac{d\bar{u}}{dy} = f(y, \rho, \bar{\tau}_s) \quad (18.48)$$

or, if we introduce u_τ ,

$$\frac{d\bar{u}}{dy} = f(y, u_\tau). \quad (18.49)$$

The only dimensionally acceptable form of equation (18.49) is

$$\frac{y}{u_\tau} \frac{d\bar{u}}{dy} = \frac{1}{\kappa} \quad (18.50)$$

or

$$y^+ \frac{du^+}{dy^+} = \frac{1}{\kappa} \quad (18.51)$$

where κ is a constant, known as **von Kármán's constant**.

Equation (18.51) can be integrated to give

$$u^+ = \frac{1}{\kappa} \ln y^+ + B \quad (18.52)$$

where B is also a universal constant. The velocity distribution represented by equation (18.52) is known as the **log law** and has been confirmed experimentally with the values¹⁷⁸ $\kappa = 0.4$, and $B = 5.5$.

An approximate indication of the sublayer thickness, δ_{SUB} , results from determining the value of y^+ at which the sublayer profile, represented by equation (18.46), has the same value of u^+ as given by the log law. The result is

$$\frac{u_\tau \delta_{SUB}}{\nu} = \delta_{SUB}^+ = 11. \quad (18.53)$$

This value is obviously much greater than $\delta_{SUB}^+ = 5$ given by equation (18.47) and which represents the wall distance at which the velocity distribution begins to depart from $u^+ = y^+$.

Although the log law was arrived at primarily using dimensional arguments, it can also be deduced using primitive turbulence modelling. In equation (18.36), the momentum equation for a two-dimensional, turbulent boundary layer, the only additional term, compared with equation (17.4) for a laminar boundary layer, is the Reynolds shear stress $\bar{\tau}_T = -\rho \overline{u'v'}$. A natural first step in attempting to account for $-\rho \overline{u'v'}$, first made by Boussinesq in 1877

¹⁷⁸ Slightly different values are sometimes quoted: $\kappa = 0.41$, and $B = 5.0$, and there is evidence that κ and B are weakly dependent upon Reynolds number.

(two decades before Reynolds introduced the idea of time averaging), was to assume that this quantity behaved in an analogous way to that for molecular shear, i.e.

$$\bar{\tau}_T = -\rho \overline{u'v'} = \mu_T \frac{\partial \bar{u}}{\partial y}, \quad (18.54)$$

which defines the quantity μ_T known as the **eddy viscosity**.

As we stated in Section 18.5, the earliest example of turbulence modelling was probably Prandtl's suggestion that, by analogy with the small-scale random motion of molecules in a gas (kinetic theory), the large-scale random movements of fluid elements (i.e. the eddies) in turbulent motion leads to a transverse exchange of momentum. If this exchange occurs over an average distance l_M , which has become known as the **mixing length**, then

$$\mu_T = \rho l_M^2 \left| \frac{\partial \bar{u}}{\partial y} \right|. \quad (18.55)$$

One way of quantifying Prandtl's idea is to assume that the **root-mean-square values** of u' and v' are approximated by

$$\sqrt{u'^2} \approx \sqrt{v'^2} \approx l_M \frac{\partial \bar{u}}{\partial y} \quad (18.56)$$

so that

$$-\overline{u'v'} \approx \sqrt{u'^2} \sqrt{v'^2} \approx l_M^2 \frac{\partial \bar{u}}{\partial y} \left| \frac{\partial \bar{u}}{\partial y} \right| = \nu_T \left| \frac{\partial \bar{u}}{\partial y} \right|. \quad (18.57)$$

The modulus sign has been introduced to ensure that the Reynolds shear stress and the velocity gradient have the same sign. In practice, it is found that, for turbulent flows in which the mean velocity is asymmetric about a maximum, there is a small region where $-\overline{u'v'}$ and $\partial \bar{u} / \partial y$ are opposite in sign, but this is of little consequence. By analogy with ν , the quantity ν_T is termed the **kinematic eddy viscosity**.

In the vicinity of a solid surface over which there is turbulent flow, it is reasonable to assume that l_M is proportional to y , i.e.

$$l_M = \kappa y \quad (18.58)$$

where, at this stage, κ is simply a constant although equation (18.60) below shows that it can be identified as **von Kármán's constant**, introduced above.

If we substitute for l_M from equation (18.58) in equation (18.57), and assume that $-\rho \overline{u'v'} = \bar{\tau}_S$, then we have

$$\kappa y \frac{\partial \bar{u}}{\partial y} = \sqrt{\frac{\bar{\tau}_S}{\rho}} = u_\tau \quad (18.59)$$

which can be rewritten as

$$y^+ \frac{du^+}{dy^+} = \frac{1}{\kappa} \quad (18.60)$$

which is identical to equation (18.51) and so again leads to the **log-law** velocity distribution, equation (18.52).

18.7.3 Buffer layer

There is no simple theory covering the near-wall range $5 < y^+ < 30$, which is intermediate between the viscous sublayer and the log-law region, often called the buffer layer. A formula suggested by Spalding (1961), which has equation (18.46) as the asymptote for $y^+ \rightarrow 0$, and which asymptotes to equation (18.52) at large y^+ is

$$y^+ = u^+ + e^{-\kappa B} \left[e^{\kappa u^+} - 1 - \kappa u^+ - \frac{1}{2} (\kappa u^+)^2 - \frac{1}{6} (\kappa u^+)^3 \right]. \quad (18.61)$$

The negative terms within square brackets can be regarded as correction terms, which are subtracted from the log-law equation in the form

$$y^+ = e^{-\kappa B} e^{\kappa u^+} = e^{-\kappa B} \left[1 + \kappa u^+ + \frac{1}{2} (\kappa u^+)^2 + \frac{1}{6} (\kappa u^+)^3 + \frac{1}{24} (\kappa u^+)^4 + \dots \right]. \quad (18.62)$$

Equations (18.46), (18.52), and (18.61) are all plotted on semi-logarithmic coordinates in Figure 18.1, together with a power-law equation with $A = 8.75$, and $m = 7$ (see Subsection 18.13.3). Spalding's formula has been shown to be an accurate fit to measured velocity distributions for pipe-flow data. The discrepancy between the power-law equation and the log law for $y^+ < 100$ is exaggerated by the logarithmic scale for the abscissa.

Van Driest (1956) suggested that, to account for the viscous sublayer, equation (18.58) for the mixing length should be modified by a so-called **damping factor**

$$l_M = \kappa y \left(1 - e^{-y^+/C} \right) \quad (18.63)$$

where the empirical constant C is usually given the value 26 if the streamwise pressure gradient is zero. If equation (18.63) is substituted in equation (18.57), numerical integration, for a constant-stress layer, results in a velocity distribution close to that corresponding

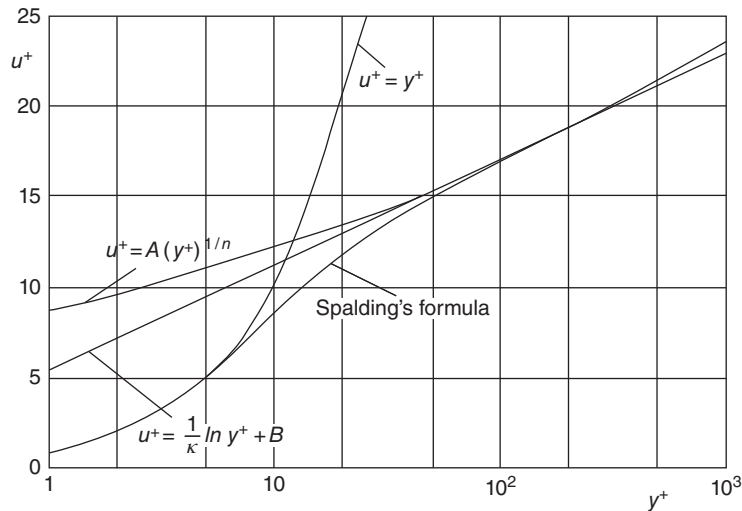


Figure 18.1 Distributions of mean velocity for near-wall turbulent flow

with Spalding's equation (18.61) but has the advantage that, if C is appropriately modified, pressure-gradient and other effects, such as transpiration, can be incorporated.

18.7.4 Outer layer and the Law of the Wake

Coles (1956) observed that, as the free stream is approached, experimentally determined velocity profiles within a turbulent boundary layer increasingly depart from the log law, particularly if there is an adverse pressure gradient, i.e. static pressure increasing with streamwise distance along the surface over which the boundary layer is developing. He showed that a good fit to the data is given by a composite in which a so-called **wake function**¹⁷⁹ $f(\eta)$ is added to the log law

$$u^+ = \frac{1}{\kappa} \ln y^+ + B + \frac{2\Pi}{\kappa} f(\eta) \quad (18.64)$$

where the **wake-strength parameter** Π increases in an adverse pressure gradient. The variable $\eta = y/\delta$, δ being the boundary-layer thickness, and the wake function $f(\eta)$ has a sigmoidal form normalised such that $f(0) = 0$ and $f(1) = 1$. A simple equation which adequately represents the wake function is¹⁸⁰

$$f(\eta) = 3\eta^2 - 2\eta^3. \quad (18.65)$$

The ratios between δ and the integral parameters displacement thickness δ^* (equation ((17.44)) and momentum-deficit thickness θ (equation (17.61)) were defined in Section 17.3. These ratios, evaluated using equation (18.64) combined with equation (18.65), are given by

$$\frac{\delta^*}{\delta} = \frac{(1 + \Pi)}{\kappa} \sqrt{\frac{c_f}{2}} \quad (18.66)$$

and

$$\frac{\theta}{\delta} = \frac{\delta^*}{\delta} - \frac{F(\Pi)}{\kappa^2} \frac{c_f}{2} \quad (18.67)$$

where

$$F(\Pi) = \frac{52}{35} \Pi^2 + \frac{19}{6} \Pi + 2 \quad (18.68)$$

and c_f is the skin-friction coefficient defined by

$$c_f = \frac{\overline{\tau_s}}{\frac{1}{2} \rho U_\infty^2}. \quad (18.69)$$

The shape factor H then follows as

$$\frac{1}{H} = \frac{\theta}{\delta^*} = 1 - \frac{F(\Pi)}{(1 + \Pi)\kappa} \sqrt{\frac{c_f}{2}} \quad (18.70)$$

¹⁷⁹ Coles used the term 'wake' because the shape of the function $f(\eta)$ resembles the velocity-defect distribution in a turbulent wake.

¹⁸⁰ Another equation for the wake function which is a good fit to the data is $f(\eta) = \sin^2(\pi\eta/2)$ but the cubic form has the advantage that the algebra involved in determining such quantities as δ^* and θ is appreciably simpler.

which confirms, as was the case for a laminar boundary layer, that $H > 1$. What is also suggested by equation (18.70) is that, given the dependence on the skin-friction coefficient, H will be Reynolds-number dependent.

Another important result, independent of the form of the wake function, is a consequence of evaluating equation (18.64) at the edge of the boundary layer, $y = \delta$, where $\bar{u} = U_\infty$

$$\sqrt{\frac{2}{c_f}} = \frac{1}{\kappa} \ln \left(\frac{U_\infty \delta}{\nu} \sqrt{\frac{c_f}{2}} \right) + B + \frac{2\Pi}{\kappa} \quad (18.71)$$

wherein we have made use of the identities

$$U_\infty^+ = \sqrt{\frac{2}{c_f}} \quad \text{and} \quad \delta^+ = \frac{u_\tau \delta}{\nu} = \frac{U_\infty \delta}{\nu} \sqrt{\frac{c_f}{2}}. \quad (18.72)$$

For boundary layers subjected to an adverse pressure gradient, experimental measurements increasingly depart from the log law as the pressure-gradient parameter¹⁸¹

$$\lambda = \frac{\delta}{\tau_s} \frac{dp}{dx} \quad (18.73)$$

is increased ($\lambda > 10$ corresponds with a strong adverse pressure gradient). For weak favourable pressure gradients ($\lambda < 0$) the wake strength is low so that the log-law equation, equation (18.52), applies throughout the near-wall region, i.e. for a boundary layer this means for $y \leq \delta$, while for pipe flow $y \leq R$.

ILLUSTRATIVE EXAMPLE 18.1

Use equation (18.64) with the wake function given by equation (18.65) to show that the ratio of the displacement thickness δ^* to the boundary-layer thickness δ for a turbulent boundary layer is given by

$$\frac{\delta^*}{\delta} = \frac{(1 + \Pi)}{\kappa} \sqrt{\frac{c_f}{2}}$$

where $c_f/2$ is the local skin-friction coefficient and Π is the wake-strength parameter.

Solution

The definition of the displacement thickness is

$$\delta^* = \int_0^\delta \left(1 - \frac{\bar{u}}{U_\infty} \right) dy.$$

The mean velocity is approximated by

$$u^+ = \frac{1}{\kappa} \ln y^+ + B + \frac{2\Pi}{\kappa} f(\eta)$$

¹⁸¹ Note that the pressure gradient λ defined here is different from those defined for both Poiseuille flow λ_p , equation (16.52), and a laminar boundary layer, equation (17.97).

where the wake function is given by

$$f(\eta) = 3\eta^2 - 2\eta^3.$$

If we substitute for \bar{u} in the definition of δ^* we have

$$\begin{aligned}\delta^* &= \delta - \frac{\nu}{u_\tau U_\infty^+} \int_0^{\delta^+} \left(\frac{1}{\kappa} \ln y^+ + B \right) dy^+ - \frac{2\Pi\delta}{\kappa U_\infty^+} \int_0^1 (3\eta^2 - 2\eta^3) d\eta \\ &= \delta - \frac{\nu}{u_\tau U_\infty^+} \left(\frac{\delta^+}{\kappa} \ln \delta^+ - \frac{\delta^+}{\kappa} + B\delta^+ \right) - \frac{\Pi\delta}{\kappa U_\infty^+} \\ &= \frac{(\Pi + 1)\delta}{\kappa U_\infty^+} = \frac{(\Pi + 1)\delta}{\kappa} \sqrt{\frac{c_f}{2}}.\end{aligned}$$

18.8 Fully-developed turbulent flow through a smooth circular pipe

For fully-developed turbulent flow through a smooth circular pipe, velocity-profile measurements show that the wake strength Π is small so that equation (18.64) with $\Pi = 0$, i.e. the log-law equation, equation (18.52), is a good approximation to the mean-velocity distribution

$$u^+ = \frac{1}{\kappa} \ln y^+ + B.$$

We can use this equation to calculate a **bulk-average** (or **spatial average**) velocity \bar{V} for fully-developed flow through a pipe of radius R (diameter D) through

$$\dot{Q} = \pi R^2 \bar{V} = \int_0^R \bar{u} 2\pi r dr \quad (18.74)$$

where \dot{Q} is the volumetric flowrate and r is the radial distance from the pipe centreline. It should be noted that we have neglected not only the wake component of the velocity distribution but also the contribution of the viscous sublayer. The latter approximation is increasingly valid as the pipe Reynolds number increases (see Self-assessment problem 18.2).

Since $r = R - y$, where y is the distance from the pipe wall, equation (18.74) leads to

$$\frac{1}{2} \bar{V} R^2 = R \int_0^R \bar{u} dy - \int_0^R \bar{u} y dy$$

which can be transformed into

$$\frac{u_\tau \bar{V} R^2}{2\nu^2} = R^+ \int_0^{R^+} u^+ dy^+ - \int_0^{R^+} u^+ y^+ dy^+. \quad (18.75)$$

If we substitute for u^+ from equation (18.52), we find, after simplification,

$$\bar{V}^+ = \frac{1}{\kappa} \ln R^+ + B - \frac{3}{2\kappa} \quad (18.76)$$

where $\bar{V}^+ = \bar{V}/u_\tau$.

If we define a friction factor f_F as in Section 16.2 (the Fanning friction factor, equation (16.16)), i.e.

$$\frac{f_F}{2} = \frac{\tau_S}{\rho \bar{V}^2} = \left(\frac{u_\tau}{\bar{V}} \right)^2 \quad (18.77)$$

then equation (18.76) leads to

$$\sqrt{\frac{2}{f_F}} = \frac{1}{\kappa} \ln \left(\frac{1}{2} \sqrt{\frac{f_F}{2}} Re_D \right) + B - \frac{3}{2\kappa} \quad (18.78)$$

where Re_D is the Reynolds number based upon \bar{V} and D .

This is quite a remarkable result—a friction-factor equation which we have arrived at without direct reference to the equations of motion. With $\kappa = 0.41$, and $B = 5.0$, equation (18.78) gives

$$\sqrt{\frac{2}{f_F}} = 2.439 \ln \left(\sqrt{\frac{f_F}{2}} Re_D \right) - 0.349$$

which is very close to a correlation, valid for $Re_D > 4 \times 10^3$, based upon experimental data¹⁸²

$$\sqrt{\frac{2}{f_F}} = 2.457 \ln \left(\sqrt{\frac{f_F}{2}} Re_D \right) + 0.292. \quad (18.79)$$

ILLUSTRATIVE EXAMPLE 18.2

Air at 25 °C flows through a smooth-walled circular pipe 100 mm in diameter at a bulk velocity of 70 m/s. Calculate the Kolmogorov scales 0.5 mm from the pipe wall, assuming fully-developed turbulent flow. Use the Kármán-Nikuradse formula to calculate the friction factor.

Solution

$D = 0.1$ m, $\bar{V} = 70$ m/s, $\rho = 1.184$ kg/m³, $\mu = 1.85 \times 10^{-5}$ Pa · s, and $y = 5 \times 10^{-4}$ m.

The Reynolds number $Re_D = 1.184 \times 70 \times 0.1 / (1.85 \times 10^{-5}) = 4.48 \times 10^5$, which confirms that the flow is turbulent (i.e. $Re_D > 4 \times 10^3$).

The Kármán-Nikuradse formula is

$$\sqrt{\frac{2}{f_F}} = 2.457 \ln \left(\sqrt{\frac{f_F}{2}} Re_D \right) + 0.292$$

from which the Fanning friction factor $f_F/2 = 1.678 \times 10^{-3}$.

The surface shear stress is then $\tau_S = \rho \bar{V}^2 f_F/2 = 9.734$ Pa so that the friction velocity $u_\tau = \sqrt{\tau_S/\rho} = 2.867$ m/s.

The distance from the surface y in wall units is $y^+ = \rho u_\tau y / \mu = 91.75$.

¹⁸² Equation (18.79) is known as the **Kármán-Nikuradse equation**, although according to White (2005) it was originally suggested by Prandtl in 1935. It is sometimes stated in terms of log-base 10 and the Darcy friction factor ($f_D = 8f_F/2$) (see Self-assessment problem 18.9).

The Kolmogorov scales are then calculated as follows from equation (18.33),

$$\frac{u_\tau l_K}{\nu} = (\kappa y^+)^{1/4} = 2.477 \text{ so that } l_K = 1.350 \times 10^{-5} \text{ or } 13.5 \mu\text{m},$$

from equation (18.34),

$$\frac{u_\tau^2 \tau_K}{\nu} = (\kappa y^+)^{1/2} = 6.133 \text{ so that } \tau_K = 1.166 \times 10^{-5} \text{ s or } 11.66 \mu\text{s}$$

and, from equation (18.35),

$$\frac{v_K}{u_\tau} = \frac{1}{(\kappa y^+)^{1/4}} = 0.404 \text{ so that } v_K = 1.158 \text{ m/s}.$$

Perhaps the most striking thing is how small the length and time scales are at $y^+ = 91.75$, which is just into the log-law region. At the edge of the viscous sublayer (taken as $y^+ = 11$, as we calculated earlier), the values are $l_K = 3.2 \mu\text{m}$, $\tau_K = 4.04 \mu\text{s}$, and $v_K = 1.97 \text{ m/s}$. Self-assessment problem 18.6 concerns the Kolmogorov scales for a boundary layer.

18.9 Surface roughness

So far we have dealt with turbulent shear flow over a smooth surface. Even when specially treated, all real surfaces are **hydrodynamically rough** to some degree, i.e. the near-wall flow differs from that for a smooth surface. While small-scale surface roughness has little effect on laminar flow, if the average **height of roughness elements**¹⁸³, ε , in turbulent flow is comparable with, or greater than, the thickness of the viscous sublayer δ_{SUB} then the near-wall (sublayer) velocity distribution and the surface shear stress are affected. If we now include ε in equation (18.40), we have

$$\bar{u} = f(y, \bar{\tau}_s, \rho, \mu, \varepsilon), \quad (18.80)$$

so that dimensional analysis leads to

$$\frac{\bar{u}}{u_\tau} = f\left(\frac{u_\tau y}{\nu}, \frac{u_\tau \varepsilon}{\nu}\right) \quad (18.81)$$

or

$$u^+ = f(y^+, \varepsilon^+) \quad (18.82)$$

where $\varepsilon^+ = u_\tau \varepsilon / \nu$ is the non-dimensional roughness height. Equation (18.47) shows that equation (18.82) can also be written as

$$u^+ = f\left(y^+, \frac{\varepsilon}{\delta_{SUB}}\right) \quad (18.83)$$

which confirms that it is the ratio of the roughness height to the thickness of the viscous sublayer which is important.

¹⁸³ See footnote 174 regarding the symbol ε .

It should be evident that to represent surface roughness in terms of a simple average roughness height is highly simplified and in reality the geometry of the roughness elements plays a role. Roughness may arise from the method of construction or finish of a surface (e.g. riveted, welded, roughly machined, sand blasted, etc.), it may be non-uniform or highly structured (e.g. strips or grooves), it may be a consequence of wear or deposition (e.g. calcium build-up in water pipes or rust), etc. Roughness is commonly modelled by glueing sand grains of a specified size to a surface.

Experimental studies have shown that the influence of roughness on a near-wall turbulent flow can be categorised as follows

- $\varepsilon^+ < 4$: **hydraulically** (or **hydrodynamically**) **smooth**, $\varepsilon < \delta_{SUB}$, and the roughness has no effect on the flow
- $4 < \varepsilon^+ < 60$: transitional-roughness regime
- $\varepsilon^+ > 60$: fully-rough regime where f_F is independent of Reynolds number (see equation (18.90))

Experimental data shows that the effect of roughness on the log law is a downward shift ΔB dependent upon the magnitude of ε^+ , so that

$$u^+ = \frac{1}{\kappa} \ln y^+ + B - \Delta B(\varepsilon^+) \quad (18.84)$$

where, according to White (2005), based upon **sand-grain roughness** experiments,

$$\Delta B \approx \frac{1}{\kappa} \ln(1 + 0.3\varepsilon^+). \quad (18.85)$$

If ΔB from equation (18.85) is substituted into equation (18.84) then, for $0.3\varepsilon^+ \gg 1$, we have

$$u^+ = \frac{1}{\kappa} \ln \left(\frac{y^+}{0.3\varepsilon^+} \right) + B = \frac{1}{\kappa} \ln \left(\frac{y}{\varepsilon} \right) + B - \frac{1}{\kappa} \ln 0.3 = \frac{1}{\kappa} \ln \left(\frac{y}{\varepsilon} \right) + 7.94 \quad (18.86)$$

where we have assumed $\kappa = 0.41$, and $B = 5$.

The principal significance of equation (18.86) is that for large values of the non-dimensional roughness height ε^+ the velocity distribution retains its logarithmic form but loses its dependence on viscosity.

18.10 Fully-developed turbulent flow through a rough-surface circular pipe

As for a smooth pipe, the velocity distribution for fully-developed turbulent flow through a pipe with a rough surface can be used to determine an equation for the bulk-average flow velocity, which can be rearranged to give a skin-friction formula. This is left as an exercise for the reader. A useful formula, devised by Colebrook (1939), for pipes with surface roughness representative of commercially available pipes is¹⁸⁴

¹⁸⁴ Equation (18.87) is usually referred to as the **Colebrook-White formula**.

$$\frac{1}{\sqrt{f_D}} = -2 \log_{10} \left(\frac{2.51}{Re_D \sqrt{f_D}} + \frac{\varepsilon}{3.7D} \right). \quad (18.87)$$

where $f_D = 8\tau_s/\rho \bar{V}^2$ is the Darcy friction factor. The ratio ε/D is referred to as **relative roughness** and typically falls within the range $10^{-5} < \varepsilon/D < 0.05$. In terms of the natural logarithm and the Fanning friction factor $f_F = f_D/4$, equation (18.87) transforms to

$$\sqrt{\frac{2}{f_F}} = -2.457 \ln \left(\frac{0.887}{Re_D} \sqrt{\frac{2}{f_F}} + \frac{\varepsilon}{3.7D} \right). \quad (18.88)$$

For a hydraulically smooth pipe, $\varepsilon = 0$, and equation (18.88) reduces to

$$\sqrt{\frac{2}{f_F}} = 2.457 \ln \left(Re_D \sqrt{\frac{f_F}{2}} \right) + 0.295 \quad (18.89)$$

which is very close to the empirical Kármán-Nikuradse equation (18.79).

For a fully-rough pipe, where $\varepsilon/D \gg 1/Re_D \sqrt{f_F}$, equation (18.88) leads to

$$\sqrt{\frac{2}{f_F}} = -2.457 \ln \left(\frac{\varepsilon}{D} \right) + 3.215 \quad (18.90)$$

and we see that f_F is independent of Re_D and so also of viscosity. The corresponding flow is referred to as **wholly** or **completely turbulent** because the viscous sublayer plays no role.

An equation which is more convenient to use than the Colebrook-White formula is

$$\sqrt{\frac{2}{f_F}} = -2.211 \ln \left[\frac{6.9}{Re_D} + \left(\frac{\varepsilon}{3.7D} \right)^{1.11} \right] \quad (18.91)$$

which is based upon a formula suggested by Haaland (1983).

A diagram in which the Fanning (or Darcy) friction factor is plotted versus pipe Reynolds number Re_D on logarithmic scales for a range of values of the relative roughness height ε/D , calculated from the Colebrook-White equation (18.87), is known as a **Moody chart** (Moody (1944)). Figure 18.2 is a version of the Moody chart for values of ε/D in the range 10^{-5} to 0.05, as well as 0. Equation (16.40) for fully-developed laminar flow through a circular pipe, $f_F Re_D = 16$, is included in Figure 18.2 for reference.

Various sources of roughness were identified in Section 18.9. Typical values for the roughness height ε are listed in Appendix 5 but should be regarded as no more than guidance to the order of magnitude of the average height of roughness elements likely to be encountered in practice.

The lower limit for the validity of the Colebrook-White formula is usually taken as $Re_D = 4 \times 10^3$, while the upper limit of equation (16.40), for fully-developed laminar pipe flow, is about $Re_D = 2 \times 10^3$. In the **transition region** $2 \times 10^3 < 4 \times 10^3$ (omitted from Figure 18.2) the flow becomes unsteady and there is no simple relationship between f_F and Re_D . From a practical point of view, this region is best avoided if a steady flow is required with predictable flow behaviour.

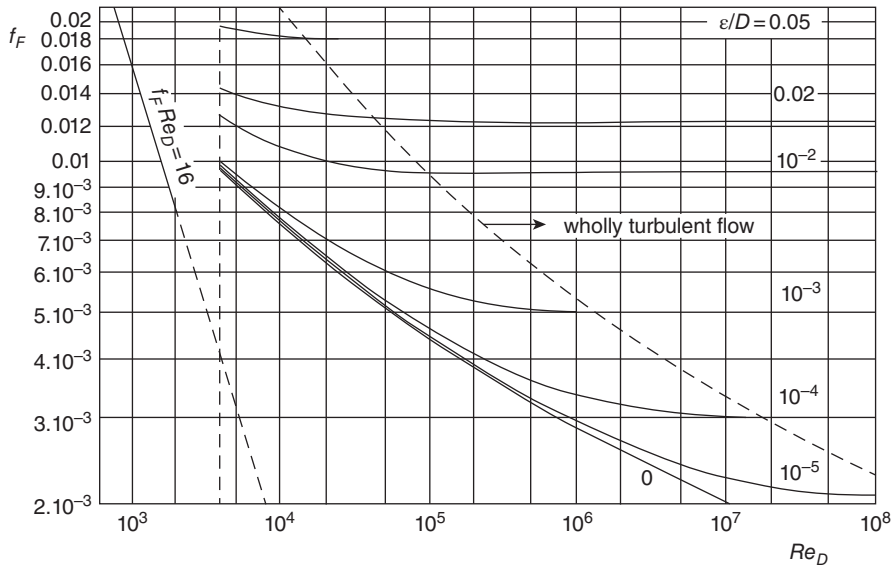


Figure 18.2 Moody chart: Fanning friction factor f_F versus Reynolds number Re_D for flow through pipes with relative roughness ε/D (logarithmic scales)

18.11 Minor losses in pipe systems

For fluid flow through any practically realistic **pipe system**, in addition to the **stagnation-pressure losses** due to surface friction, termed the **major losses**, account has to be taken of so-called **minor losses**¹⁸⁵, the main causes of which are

- disturbances at the pipe entrance and exit
- sudden increases or decreases in cross section
- gradual increases in cross section (diffusers)
- fully or partially open valves
- bends, elbows, tee junctions, and other pipe fittings

Since pressure can be regarded as a form of energy (see Subsection 7.5.1), the term **pressure loss** is misleading as the mechanical energy concerned is simply converted into heat, and no energy is actually lost. However, the term is well established and so will continue to be used here. From the list above it is apparent that pressure losses are associated primarily with friction, area change, and direction change.

The majority of flows of engineering significance have sufficiently high Reynolds numbers that they are turbulent. Commercial software packages, based upon a wide variety of turbulence models, are now available for the calculation to acceptable levels of accuracy of the flow characteristics of pipe systems, including velocity, pressure, and turbulence-intensity distributions, as well as overall pressure loss. However, if all that is needed is the calculation of overall stagnation-pressure loss from inlet to outlet of a system, it is usually adequate to characterise each component (i.e. **pipe fitting**) in the system using an empirical **loss coefficient** K .

¹⁸⁵ In spite of the names, it is often the case that in practice the minor losses exceed the major losses.

For an incompressible fluid of density ρ , the definition of K is

$$K = \frac{\Delta p_0}{\frac{1}{2}\rho\bar{V}^2} \quad (18.92)$$

where Δp_0 is the loss in stagnation pressure across an individual component for a bulk flow velocity \bar{V} at its inlet. If there is no change in cross-sectional area from inlet to outlet of a component, then the changes in static and stagnation pressure are equal.

Although K depends primarily on the basic shape of a component, details of the internal geometry are also important. For example, for a sudden contraction K can be reduced from 0.5 to 0.02 by appropriate rounding of the inlet. In the case of a bend¹⁸⁶, the pressure loss is a consequence of the bend radius (which may not be constant), which gives rise to **secondary flows** (counter-rotating vortices) due to centripetal acceleration. The loss may also be associated with flow separation on the low-radius side and affected by the cross-section shape, internal surface roughness, method of installation (e.g. flanged or threaded), which is often unstated but has a major influence, and the Reynolds number (K typically decreases as the Reynolds number increases). Loss coefficients for all fittings are also affected by the upstream flow conditions, higher losses being associated with a fully-developed upstream flow rather than a uniform flow. For large bends with a rectangular cross section, as is typical for a wind or water tunnel, it is usual to incorporate a **cascade** of **guidevanes** (see Section 10.9) to reduce losses and improve flow quality.

As will be shown in Subsection 18.11.1, for a sudden enlargement a good estimate for the loss coefficient K_{SE} is given by an analysis based upon the linear momentum equation. A similar analysis (Subsection 18.11.2) for a sudden contraction requires a correction factor, however. Subject to the influences mentioned in the previous paragraph, guideline values of K for various elbows and **tee junctions** are listed in Table 18.1.

For more accurate values it is necessary to consult the manufacturer's literature for a given fitting. A regular elbow, a long-radius elbow, a line-flow tee junction, and a branch-flow tee junction are shown schematically in Figure 18.3.

18.11.1 Sudden enlargement and Borda-Carnot equation

In Section 10.5 it was shown that the changes in static p and stagnation pressure p_0 for flow through a **sudden enlargement** can be calculated by applying the linear momentum equation to the flow, which leads to

$$p_2 - p_1 = \frac{\dot{m}^2}{\rho A_2} \left(\frac{1}{A_1} - \frac{1}{A_2} \right) \quad (18.93)$$

¹⁸⁶ The terms **pipe bend** and **pipe elbow** tend to be used interchangeably and inconsistently. Both refer to a component which joins two sections of pipe where there is an angle between the two. It is sometimes said that all elbows are bends but not all bends are elbows. The difference is that the term bend is generic and describes an offset or change in the direction of piping, while an elbow is a component prefabricated to a standard, the bend angle usually being 45°, 90°, or 180°, although any angle is clearly possible. An elbow with an angle of 180° is referred to as a **return bend**. If the nominal (internal) pipe diameter is D , the bend radius for a **standard** (or **regular** or **short-radius**) elbow is $1D$, while for a **long-radius elbow** the standard bend radius is $1.5D$. Other common choices for the radius of an elbow are $3D$ and $5D$.

Table 18.1 Loss coefficients (K) for pipe elbows and tee junctions

Elbows	
45° standard radius, flanged	0.2
45° standard radius, threaded	0.4
45° long radius, flanged	0.2
90° standard radius, flanged	0.3
90° standard radius, threaded	1.5
90° long radius, flanged	0.2
90° long radius, threaded	0.7
180° standard radius, flanged	0.2
180° standard radius, threaded	1.5
Tee junctions	
Line flow, flanged	0.2
Line flow, threaded	0.9
Branch flow entering line	1.3
Line flow entering branch	1.5

and the **Borda-Carnot equation**

$$p_{0,1} - p_{0,2} = \frac{\dot{m}^2}{2\rho} \left(\frac{1}{A_1} - \frac{1}{A_2} \right)^2 \quad (18.94)$$

where ρ is the (constant) fluid density, \dot{m} is the mass flowrate, A is the cross-sectional area, and the subscripts 1 and 2 refer to the regions upstream and downstream of the enlargement, respectively.

If the upstream diameter is d , and the downstream diameter is D , it is straightforward to show from equation (18.94) that for a sudden enlargement the loss coefficient K_{SE} is given by

$$K_{SE} = \frac{\Delta p_0}{\frac{1}{2}\rho\bar{V}_1^2} = \left[1 - \left(\frac{d}{D} \right)^2 \right]^2. \quad (18.95)$$

For flow from a duct with area issuing into the surroundings, equation (18.95) with $D \rightarrow \infty$ leads to $K_{SE} = 1$, i.e. the stagnation-pressure loss is equal to the dynamic pressure upstream of the contraction.

The variation of K_{SE} with diameter ratio is shown in Figure 18.5.

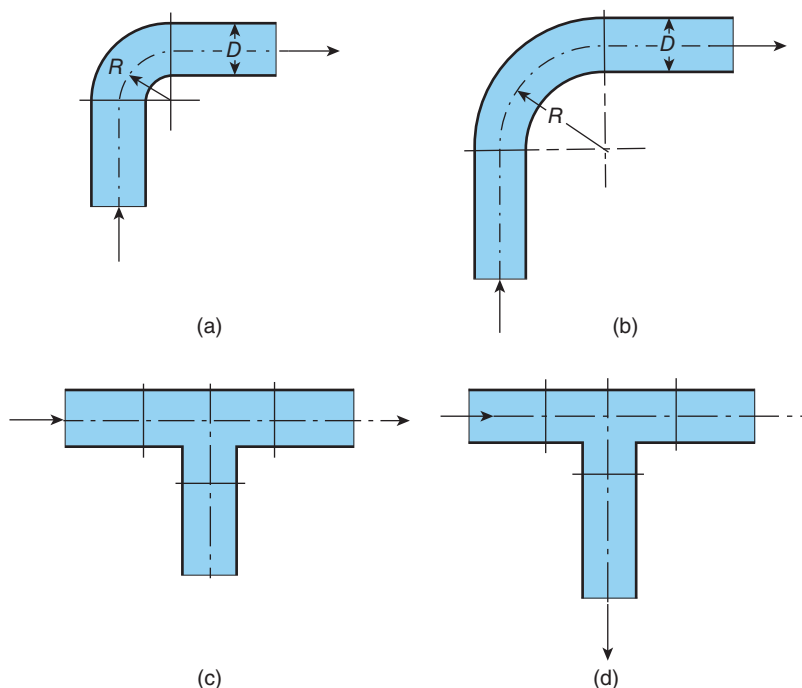


Figure 18.3 Pipe fittings: (a) regular pipe elbow (b) long-radius pipe elbow (c) line-flow tee junction (d) branch-flow tee junction

18.11.2 Sudden contraction

As shown in Figure 18.4, flow through a **sudden contraction** is complicated by the fact that the flow separates at the corner of the contraction, in the same way as for an **orifice-plate flowmeter**. Account then has to be taken of the occurrence of a **vena contracta** downstream of the contraction, the cross-sectional area of which (A_V) is unknown. If we treat the flow

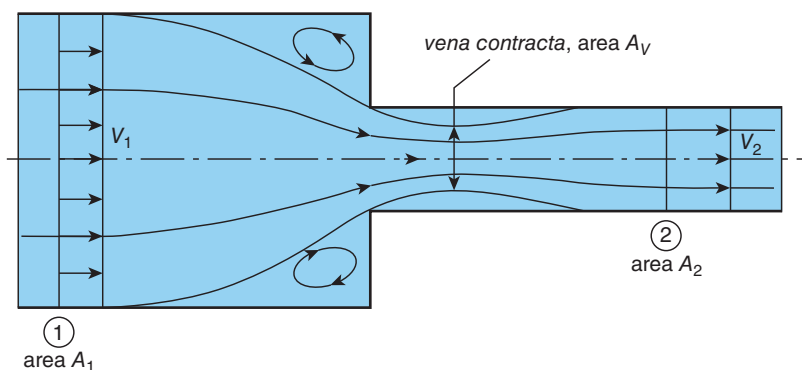


Figure 18.4 Schematic diagram of flow through a sudden contraction, showing separated flow and the *vena contracta*

between the *vena contracta* and the downstream pipe as though it were a sudden enlargement, and also assume that there is zero loss in stagnation pressure between the upstream region so that $p_{0,V} = p_{0,1}$, then we can use the Borda-Carnot equation, equation (18.94), to calculate the loss in stagnation pressure as

$$p_{0,1} - p_{0,2} = \frac{\dot{m}^2}{2\rho} \left(\frac{1}{A_V} - \frac{1}{A_2} \right)^2 \quad (18.96)$$

It is usual for a sudden contraction to refer to the bulk-average velocity in the downstream pipe, \bar{V}_2 , so that

$$\frac{p_{0,1} - p_{0,2}}{\frac{1}{2}\rho\bar{V}_2^2} = \left(\frac{A_2}{A_V} - 1 \right)^2 = K_{SC} \quad (18.97)$$

where K_{SC} is the loss coefficient for the sudden contraction. Since the ratio A_V/A_2 depends upon the overall contraction ratio A_2/A_1 so does the loss coefficient. For a contraction with sharp edges, White (2011) recommends the empirical formula

$$K_{SC} = 0.42 \left[1 - \left(\frac{d}{D} \right)^2 \right] \quad (18.98)$$

where d is the diameter of the downstream pipe and D is the diameter of the upstream pipe. Other writers suggest that the coefficient should be 0.5 rather than 0.42.

The variation of K_{SC} with diameter ratio is shown in Figure 18.5. Rounding the contraction edges reduces K_{SC} considerably: by about 50% if the edge radius is $0.06D$, and 95% for $0.25D$.

18.11.3 Total stagnation-pressure loss

For a pipe of diameter D and length L with N fittings, the overall stagnation-pressure loss $\Delta p_{0,OVERALL}$ is given by

$$\Delta p_{0,OVERALL} = \Delta p_L + \sum_{i=1}^N \Delta p_{0,i} \quad (18.99)$$

where Δp_L is the pressure loss over the pipe length and $\Delta p_{0,i}$ is the stagnation-pressure loss across the i^{th} fitting.

If f_F is the Fanning friction factor then, assuming fully-developed flow in the pipe with bulk-average velocity \bar{V} ,

$$\Delta p_L = \frac{4\tau_s L}{D} = 2\rho\bar{V}^2 f_F \frac{L}{D} \quad (18.100)$$

where τ_s is the surface shear stress within the pipe. If \bar{V} , and hence Re_D , are known, the Fanning friction factor can be calculated from the Colebrook-White equation, from Section 18.10, or obtained from the Moody chart.

If the pipe diameter changes between fittings, then the pressure loss in each section has to be calculated separately to account for the changes in \bar{V} . Clearly, if a section is too short, the assumption of fully-developed flow (implied by equation (18.100)) becomes invalid.

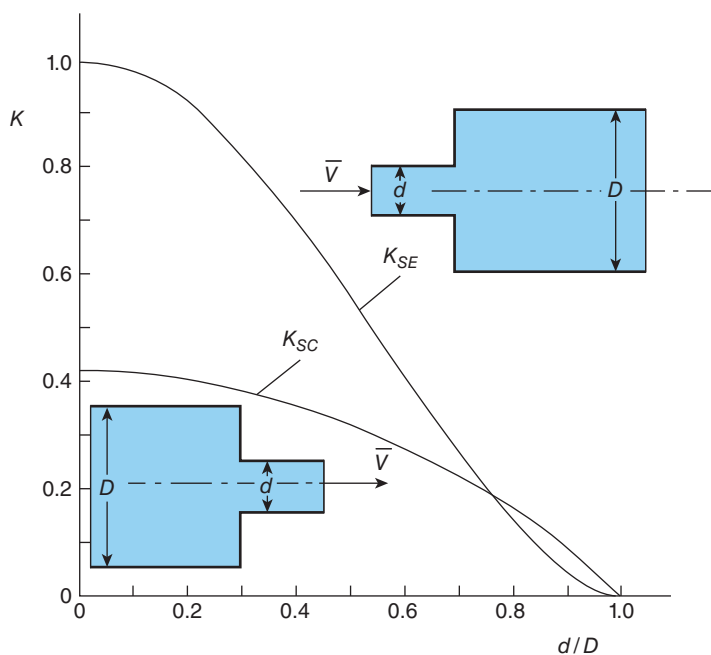


Figure 18.5 Variation of loss coefficient with diameter ratio d/D for (a) sudden enlargement (K_{SE}) and (b) sharp-edge sudden contraction (K_{SC}).

For fitting i we have

$$\Delta p_{0,i} = K_i \frac{1}{2} \rho \bar{V}_i^2 \quad (18.101)$$

so that, finally,

$$\Delta p_{0,OVERALL} = 2\rho \bar{V}_F^2 \frac{L}{D} + \frac{1}{2} \rho \sum_i^N K_i \bar{V}_i^2. \quad (18.102)$$

As we saw in Section 4.3, a static-pressure difference Δp can be represented in terms of the height of a column of liquid $h = \Delta p / \rho g$, the height being referred to as the head. This concept can be applied to any fluid but, in the case of gases and vapours, the density of a reference liquid, such as water, an oil, or mercury, has to be introduced. The overall pressure loss expressed in this way is referred to as a **head loss**.

ILLUSTRATIVE EXAMPLE 18.3

In a chemical plant, paraffin oil (kerosene) with a specific density of 0.804 and dynamic viscosity $1.92 \times 10^{-3} \text{ Pa} \cdot \text{s}$ is pumped between two large containers at a volumetric flowrate of $0.006 \text{ m}^3/\text{s}$ through a pipe with diameter $D = 50 \text{ mm}$ and length $L = 150 \text{ m}$. The relative roughness is 10^{-4} . Installed within the pipe are the following: a standard 90° elbow with radius D , a long-radius 90° elbow with radius $1.5 D$, both flanged, and two partially open valves with

loss coefficients 2.0 and 5.0, respectively. The flow enters the pipe through a sharp-edged entrance and leaves through a sharp-edged exit. Calculate the overall pressure difference and the pumping power required. Both containers are on the same horizontal level.

Solution

$D = 0.04 \text{ m}$, $L = 150 \text{ m}$, $\dot{Q} = 0.009 \text{ m}^3/\text{s}$, $\rho = 804 \text{ kg/m}^3$, $\mu = 1.92 \times 10^{-3} \text{ Pa} \cdot \text{s}$, $\varepsilon/D = 10^{-4}$, $K_1 = 0.42$ (pipe inlet), $K_2 = 2.0$ (first valve), $K_3 = 0.3$ (flanged 90° standard elbow, $R_3 = D$), $K_4 = 0.2$ (flanged 90° long-radius elbow, $R_4 = 1.5 D$), and $K_5 = 5.0$ (second valve). Mean velocity in pipe $\bar{V} = 4\dot{Q}/\pi D^2 = 7.162 \text{ m/s}$.

Reynolds number $Re_D = \rho \bar{V} D / \mu = 1.2 \times 10^5$.

From the Moody chart a first estimate for the Fanning friction factor is $f_F = 4.5 \times 10^{-3}$.

With $f_F = 4.5 \times 10^{-3}$ as an initial estimate, from the Colebrook-White equation $f_F = 4.475 \times 10^{-3}$.

The sum of the five loss coefficients $\sum K_i = 7.92$.

The overall stagnation-pressure difference $\Delta p_{0,OVERALL}$ is given by

$$\Delta p_{0,TOTAL} = 2\rho \bar{V}^2 f_F \frac{L}{D} + \frac{1}{2}\rho \sum_i^K K_i \bar{V}^2 = 1.547 \text{ MPa}$$

and the required pumping power $P = \dot{Q} \Delta p_{0,OVERALL} = 13.92 \text{ kW}$.

The electrical power supplied to the pump would need to be about 25% higher, given that pumps are less than 100% efficient.

18.12 Momentum-integral equation

In Section 17.5 we showed that, by considering the forces acting on a control volume of infinitesimal width in the streamwise direction, and the flowrates of streamwise momentum into and out of the control volume, we can derive von Kármán's **momentum-integral equation** for a two-dimensional, constant-property, laminar boundary layer

$$\frac{c_f}{2} = \frac{d\theta}{dx} + (H + 2) \frac{\theta}{U_\infty} \frac{dU_\infty}{dx}. \quad (17.86)$$

This equation can also be derived by formal integration across the boundary layer of the boundary-layer form of the Navier-Stokes equations. The same approach can be applied to the Reynolds-averaged equations for a turbulent boundary layer, with the result

$$\frac{c_f}{2} = \frac{d\theta}{dx} + (H + 2) \frac{\theta}{U_\infty} \frac{dU_\infty}{dx} + \frac{1}{U_\infty^2} \frac{d}{dx} \int_0^\infty (\overline{u'^2} - \overline{v'^2}) dy \quad (18.103)$$

although it is usual to assume that the integral involving the normal-stress terms is negligible. The momentum-integral equation for a turbulent boundary layer is then identical to that for a laminar boundary layer, although it has to be remembered that the momentum and displacement thicknesses, θ and δ^* , respectively, have to be calculated from the distribution of the mean velocity $\bar{u}(y)$ for a turbulent boundary layer.

18.13 Flat-plate boundary layer

18.13.1 Wall-plus-wake velocity profile

From the wall-plus-wake velocity distribution, the skin-friction coefficient $c_f/2$ is given by equation (18.71)

$$\sqrt{\frac{2}{c_f}} = \frac{1}{\kappa} \ln \left(\sqrt{\frac{c_f}{2}} \frac{U_\infty \delta}{\nu} \right) + B + \frac{2\Pi}{\kappa} \quad (18.71)$$

Π being the wake parameter, and δ the boundary-layer thickness.

In Subsection 18.7.4 we showed that the momentum-deficit thickness θ corresponding to the combined log-law and law-of-the-wake velocity distribution, equation (18.64), is given by

$$\frac{\theta}{\delta} = \left(\frac{\Pi + 1}{\kappa} \right) \sqrt{\frac{c_f}{2}} - \frac{F(\Pi)}{\kappa^2} \frac{c_f}{2} \quad (18.104)$$

where

$$F(\Pi) = \frac{52}{35} \Pi^2 + \frac{19}{6} \Pi + 2 \quad (18.68)$$

so that equations (18.71) and (18.104) can be combined to eliminate δ and produce the following equation connecting the skin-friction coefficient c_f , the momentum-thickness Reynolds number, defined by $Re_\theta = U_\infty \theta / \nu$, and the wake parameter Π

$$\frac{U_\infty \theta}{\nu} = Re_\theta = \left[\Pi + 1 - F(\Pi) \frac{1}{\kappa} \sqrt{\frac{c_f}{2}} \right] \frac{e^{\kappa \sqrt{2/c_f}}}{\kappa} e^{-(B\kappa + 2\Pi)}. \quad (18.105)$$

In principle equation (18.105) can be seen as a relationship between the momentum-thickness Reynolds number Re_θ and $c_f/2$ although the form of the equation is inconvenient, and the value (or x -variation) of the wake parameter Π is, as yet, unknown.

For a zero-pressure-gradient (flat-plate) boundary layer the momentum-integral equation (18.103), neglecting the $u'^2 - \bar{v}^2$ term, reduces to

$$\frac{d\theta}{dx} = \frac{c_f}{2}. \quad (18.106)$$

Substitution for θ from equation (18.105) in equation (18.106) leads to an ordinary differential equation which can be solved to give the following equation for the streamwise Reynolds number Re_x , if the wake parameter Π is assumed to be independent of x

$$Re_x = \frac{1}{\kappa^3} \left[(\Pi + 1) \left(\frac{2\kappa^2}{c_f} - 2\kappa \sqrt{\frac{2}{c_f}} + 2 \right) - F(\Pi) \left(\kappa \sqrt{\frac{2}{c_f}} - 2 \right) \right] e^{\kappa \sqrt{2/c_f}} e^{-(B\kappa + 2\Pi)}. \quad (18.107)$$

Unfortunately, it is not possible to rearrange the equation such that c_f is an explicit function of Re_x so that, given Re_x , an iterative procedure is required to determine c_f . Also, although the algebra leading to equation (18.107) is straightforward, it is quite tedious and requires the assumption that Π is constant. For a flat-plate boundary layer a value for Π of about 0.45 is found to be a good fit to experimental data. With $\Pi = 0$ what remains of the wall-plus-wake

equation (18.64) is the log law, but even then the resulting relationships between c_f and both Re_θ and Re_x are inconvenient for further analysis.

18.13.2 Empirical drag laws

A number of purely empirical relations between c_f and Re_x , known as **drag laws**, have been proposed, one of the earliest being that suggested by Schultz-Grunow (1940) for the range $10^6 \leq Re_x \leq 10^9$

$$\frac{c_f}{2} = \frac{0.185}{(\log_{10} Re_x)^{2.584}} \quad (18.108)$$

while, more recently, White (2005) suggested

$$\frac{c_f}{2} = \frac{0.2275}{\ln^2(0.06 Re_x)}. \quad (18.109)$$

Both formulae have the merit that c_f is an explicit function of Re_x but, as we shall see in Subsection 18.13.3, it is also useful to express the skin-friction coefficient in terms of the momentum-thickness Reynolds number $Re_\theta = U_\infty \theta / \nu$.

18.13.3 Power-law velocity profile

It is straightforward to derive explicit relationships between c_f and both Re_θ and Re_x if the velocity-profile assumption (for a flat-plate boundary layer) takes the **power-law** form:

$$u^+ = A (y^+)^m \quad (18.110)$$

where A and m are constants. Such an assumption is tantamount to assuming $\Pi = 0$: as shown in Figure 18.1, with $A = 8.75$, and $m = 1/7$, equation (18.110) is close to the log law, equation (18.52), for $y^+ < 1500$.

If equation (18.110) is written in the form

$$\frac{\bar{u}}{U_\infty} = \left(\frac{y}{\delta} \right)^m = \xi^m, \quad (18.111)$$

where $\xi = y/\delta$, from the definition of θ , equation (17.46), we have

$$\frac{\theta}{\delta} = \frac{1}{\delta} \int_0^\delta \frac{\bar{u}}{U_\infty} \left(1 - \frac{\bar{u}}{U_\infty} \right) dy = \int_0^1 \xi^m (1 - \xi^m) d\xi = \frac{m}{(m+1)(2m+1)}. \quad (18.112)$$

With $m = 1/7$ equation (18.112) gives $\theta/\delta = 7/72 = 0.0972$, i.e. $\theta \ll \delta$.

According to the momentum-integral equation for a flat-plate boundary layer,

$$\frac{d\theta}{dx} = \frac{c_f}{2} \quad (18.106)$$

so that

$$\frac{c_f}{2} = \frac{m}{(m+1)(2m+1)} \frac{d\delta}{dx} = \frac{m}{(m+1)(2m+1)} \frac{dRe_\delta}{dRe_x} \quad (18.113)$$

where $Re_x = U_\infty x / \nu$, and $Re_\delta = U_\infty \delta / \nu$.

From equation (18.110) at $y = \delta$

$$U_{\infty}^+ = A (\delta^+)^m$$

which can be transformed into a skin-friction equation in terms of Re_{δ}

$$\frac{c_f}{2} = A^{-2/(m+1)} Re_{\delta}^{-2m/(m+1)}. \quad (18.114)$$

With $A = 8.75$, and $m = 1/7$, this becomes

$$\frac{c_f}{2} = 0.0225 Re_{\delta}^{-0.25}. \quad (18.115)$$

Substitution for δ from equation (18.112) allows equation (18.114) to be transformed into the required relationship between $c_f/2$ and Re_{θ}

$$\frac{c_f}{2} = A^{-2/(m+1)} \left[\frac{m}{(m+1)(2m+1)} \right]^{2m/(m+1)} Re_{\theta}^{-2m/(m+1)}. \quad (18.116)$$

With the values for A and m used above we have

$$\frac{c_f}{2} = 0.0125 Re_{\theta}^{-0.25}. \quad (18.117)$$

If equation (18.114) is used to eliminate Re_{δ} from equation (18.113) to give a differential equation for $c_f/2$, we find, after integration

$$\frac{c_f}{2} = \left[A^{-2/(3m+1)} \frac{m}{(2m+1)(3m+1)} \right]^{2m/(3m+1)} Re_x^{-2m/(3m+1)} \quad (18.118)$$

and, with $A = 8.75$, and $m = 1/7$, we have

$$\frac{c_f}{2} = 0.0288 Re_x^{-0.2}. \quad (18.119)$$

The equations for $c_f/2$ derived here from the power-law equation are less accurate than the empirical equations based directly on experimental data. They are, however, very convenient for analytical studies.

It may be remarked that this analysis of a flat-plate turbulent boundary layer is similar in a number of ways to the profile-method of analysis for a laminar boundary layer presented in Section 17.6.

ILLUSTRATIVE EXAMPLE 18.4

- Calculate the value of $c_f/2$ given by White's equation, equation (18.109), for a flat-plate turbulent boundary layer with $Re_x = 10^9$.
- Solve equation (18.107) with $\Pi = 0.45$, $\kappa = 0.41$, and $B = 5.0$ to find the value of Re_x corresponding to the value of $c_f/2$ found in part (a).
- Calculate the value of $c_f/2$ given by White's equation with the value of Re_x obtained in part (b). Comment on the results.

Solution

(a) White's equation (equation (18.109)) is

$$\frac{c_f}{2} = \frac{0.2275}{\ln^2(0.06Re_x)}.$$

With $Re_x = 10^9$ this equation gives $c_f/2 = 0.2275/\ln^2(0.06 \times 10^9) = 7.092 \times 10^{-4}$.

(b) Equation (18.107) is

$$Re_x = \frac{1}{\kappa^3} \left[(\Pi + 1) \left(\frac{2\kappa^2}{c_f} - 2\kappa \sqrt{\frac{2}{c_f}} + 2 \right) - F(\Pi) \left(\kappa \sqrt{\frac{2}{c_f}} - 2 \right) \right] e^{\kappa \sqrt{2/c_f}} e^{-(B\kappa + 2\Pi)}$$

with

$$F(\Pi) = \frac{52}{35} \Pi^2 + \frac{19}{6} \Pi + 2.$$

With $\Pi = 0.45$ we find $F(\Pi) = 3.726$. It is convenient to substitute $\beta = \kappa \sqrt{2/c_f}$ so that

$$Re_x = \frac{1}{0.41^3} [1.45(\beta^2 - 2\beta + 2) - 3.726(\beta - 2)] e^\beta e^{-(5 \times 0.41 + 0.9)}.$$

With $c_f/2 = 7.092 \times 10^{-4}$ we have $\beta = 15.40$ and, finally, $Re_x = 9.289 \times 10^8$.

(c) If we substitute the value of Re_x from part (b) into White's equation we find $c_f/2 = 7.151 \times 10^{-4}$.

Comments:

The value for Re_x found in part (b) is within 7% of 10^9 , the value used to determine $c_f/2$ from White's equation, which initially suggests a significant discrepancy. However, this value of Re_x leads to a value of $c_f/2$ within 1% of that given by White's equation, showing that the dependence of $c_f/2$ on Re_x is very weak and also that the log law plus wake function leads to a skin-friction equation which is of comparable accuracy with experimental data as represented by White's empirical equation.

18.13.4 Flat-plate boundary-layer transition

It is usually the case, unless special measures are used to 'trip' the laminar boundary layer which develops from the leading edge of a flat plate, that **transition** to turbulent flow occurs following the growth of instabilities within the boundary layer. The streamwise distance over which transition occurs is usually relatively short and it is sufficient to assume that transition occurs instantaneously once a **critical Reynolds number** is reached.

For a zero pressure-gradient boundary layer on a smooth surface, an appropriate value for the critical streamwise Reynolds number $Re_{x,C} = U_\infty x/\nu$ is 3×10^6 if the free-stream turbulence level $\bar{k}_\infty < 1.5 \times 10^{-6} U_\infty^2$, where \bar{k}_∞ is the turbulent kinetic-energy per unit mass in the **free stream** (i.e. for $y > \delta$). Experiments show that the value of $Re_{x,C}$ decreases monotonically for higher values of \bar{k}_∞ , becoming negligible for $\bar{k}_\infty > 10^{-3} U_\infty^2$. Surface roughness also leads to a

decrease in $Re_{x,C}$, a value of 5×10^5 being appropriate for a typical industrial material where low friction is important.

If we assume that the boundary layer remains laminar up to the point of transition, x_C , then, based upon the result for zero-pressure gradient tabulated in Table 17.2 in Chapter 17, the momentum thickness θ_C corresponding with x_C is given by

$$\frac{\theta_C}{x_C} \sqrt{Re_{x,C}} = 0.6641$$

from which we conclude, if $Re_{x,C} = 3 \times 10^6$, then

$$Re_{\theta,C} \approx 1150. \quad (18.120)$$

It is sometimes more convenient to present results as functions of the **momentum-thickness Reynolds number** Re_θ rather than the streamwise Reynolds number Re_x .

Once the transition-onset location x_C has been determined, the continuing development of the (now turbulent) boundary layer can be calculated as follows. If it is assumed that the transition region is short compared with the downstream stretch of turbulent boundary layer, then it is reasonable to assume that both the mass flowrate per unit width within the boundary layer \dot{m}' given by

$$\dot{m}' = \rho \int_0^\delta u \, dy$$

and the corresponding momentum flowrate per unit width \dot{M}' given by

$$\dot{M}' = \rho \int_0^\delta u^2 \, dy$$

remain unchanged across the transition region. From this it can be concluded that the momentum thickness also remains unchanged, since

$$\theta = \int_0^\delta \frac{u}{U_\infty} \left(1 - \frac{u}{U_\infty}\right) dy = \frac{\dot{m}'}{\rho U_\infty} - \frac{\dot{M}'}{\rho U_\infty^2}. \quad (18.121)$$

Assuming that the momentum thickness remains unchanged leads to the interesting conclusion that the boundary-layer thickness also changes only slightly. We found in Subsection 17.3.2 that, for a flat-plate laminar boundary layer,

$$\frac{\theta_L}{\delta} = 0.09393 \quad (17.47)$$

and, assuming the $1/7^{\text{th}}$ power-law velocity profile for a turbulent boundary layer,

$$\frac{\theta_T}{\delta} = \frac{7}{72} = 0.0972 \quad (18.122)$$

so that, at the location of transition,

$$\frac{\theta_T}{\theta_L} = 1.035.$$

This value of θ_T/θ_L is subject to many uncertainties: the value of δ_L depends upon how close to unity is the value of u/U_∞ at which it is decided that the edge of the boundary layer has

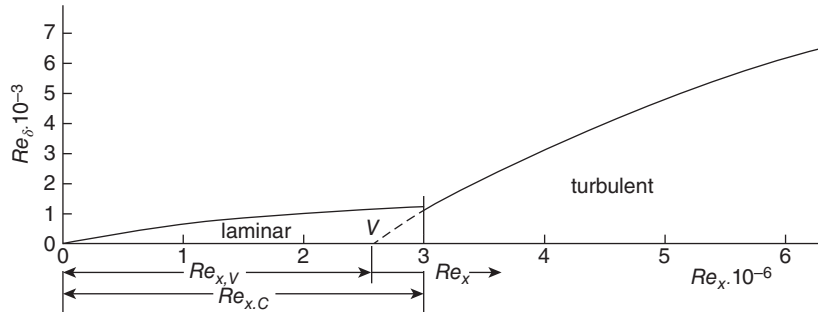


Figure 18.6 Schematic diagram of transition of a flat-plate boundary layer (note that there is a factor of 250 between the Re_x - and Re_θ -scales)

been reached (according to Table 17.1 in Chapter 17, the value of y/Δ which leads to equation (17.47) corresponds to $u/U_\infty = 0.99994$), and the value of δ_T is a consequence of the choice of the simple power-law representation of the velocity profile. Nevertheless, it is clear that the boundary-layer thickness has to adjust to accommodate the redistribution of momentum which occurs during transition.

The continuing development of the (now turbulent) boundary layer can be calculated assuming that it originates from a **virtual origin** such that the momentum thickness of the turbulent boundary layer at x_C is equal to the momentum thickness of the laminar boundary layer at that location. The flow configuration is illustrated in Figure 18.6, with the virtual origin marked by V . The more rapid growth rate of the turbulent boundary layer is clearly seen. The consideration here is a good example of the merit in specifying a transition criterion in terms of the momentum-thickness Reynolds number.

ILLUSTRATIVE EXAMPLE 18.5

A flat plate 20 m long and 5 m wide is placed in an airflow at 20 °C having a velocity of 40 m/s. The streamwise pressure gradient is zero. Assume that the boundary layer on the plate transitions from laminar to turbulent instantaneously at a location where the streamwise Reynolds number $Re_x = 3 \times 10^6$.

- (i) Calculate the streamwise location x_C at which transition occurs and the corresponding values of the momentum-thickness Reynolds number $Re_{\theta,C}$, the momentum thickness θ_C , the surface shear stress $\tau_{s,C}$, and the drag force D_L for the laminar-flow section.
- (ii) Calculate the location x_V of the virtual origin of the turbulent boundary layer, the surface shear stress at the location x_C for the turbulent boundary layer, the surface shear stress at the end of the plate $\tau_{s,E}$, and the total drag force D_T over the turbulent-flow section. Hence calculate the drag force D_E exerted by the flow on the entire plate.
- (iii) What would be the drag force if the flow were entirely laminar from the leading edge to the trailing edge of the plate?
- (iv) What would be the drag force if the flow were entirely turbulent from the leading edge of the plate?

Solution

$L = 20$ m, $W = 5$ m, $\mu = 1.82 \times 10^{-5}$ Pa · s, $\rho = 1.204$ kg/m³, $U_\infty = 40$ m/s, and $Re_C = 3 \times 10^6$. To distinguish, where appropriate, the laminar section from the turbulent section of the boundary layer we shall use the subscripts L and T , respectively, while subscript E will denote the end of the plate, and C the location of transition.

- (i) From $Re_C = 3 \times 10^6$, we have

$$x_C = \mu Re_C / (\rho U_\infty) = 1.82 \times 10^{-5} \times 3 \times 10^6 / (1.204 \times 40) = 1.134 \text{ m}.$$

For a flat-plate laminar boundary layer, from Table 17.2, $Re_\theta = 0.6641 \sqrt{Re_x}$, so that $Re_{\theta,C} = 0.6641 \sqrt{Re_{x,C}}$. We thus find $Re_{\theta,C} = 0.6641 \times \sqrt{3 \times 10^6} = 1150.3$, so that $\theta_C = \mu Re_{\theta,C} / (\rho U_\infty) = 4.347 \times 10^{-4}$ m, or 0.435 mm.

From Table 17.2, for a zero-pressure-gradient laminar boundary layer $(c_{f,L}/2)Re_\theta = 0.2205$ so that at $x = x_C$ we have $c_{f,L}/2 = 0.2205/1150.3 = 1.917 \times 10^{-4}$. Since $c_{f,L}/2 = \tau_{S,C} / \rho U_\infty^2$, we find $\tau_{S,C} = 1.204 \times 40^2 \times 1.917 \times 10^{-4} = 0.369$ Pa.

From equation (17.89), the drag force exerted over the length x_C is given by $D_C = \rho U_\infty^2 \theta_C W = 4.19$ N. The same result is arrived at by noting that, since $\tau_S \propto x^{-1/2}$ for a laminar, flat-plate boundary layer, the average wall shear stress over any length $x = 2\tau_{S,x}$, and so $D_C = 2\tau_{S,C} W x_C$.

- (ii) It is assumed that the momentum thickness for the turbulent boundary layer at the location of transition is unchanged from that for preceding the laminar boundary layer, i.e. $\theta_C = 0.435$ mm, and $Re_{\theta,C} = 1150.3$.

We shall use the symbol χ to represent streamwise distance from the virtual origin, as shown in Figure 18.6, i.e. $\chi = x - x_V$. The location of the virtual origin x_V is then found as follows. According to equations (18.117) and (18.119), for the turbulent boundary layer at the transition location,

$$\frac{c_{f,T}}{2} = 0.0125 Re_{\theta,C}^{-0.25} = 0.0288 Re_{\chi,C}^{-0.2}$$

from which we find

$$\frac{c_{f,T}}{2} = 2.146 \times 10^{-3} \text{ and } Re_{\chi,C} = 4.349 \times 10^5$$

so that

$$\chi_C = \frac{\mu}{\rho U_\infty} Re_{\chi,C} = 0.164 \text{ m and } \tau_{S,C} = \rho U_\infty^2 \frac{c_{f,T}}{2} = 4.135 \text{ Pa}.$$

Given that $\chi_C = x_C - x_V$ (see Figure 18.6), we have $x_V = x_C - \chi_C = 1.134 - 0.164 = 0.970$ m. The distance from the virtual origin to the end of the plate $\chi_E = L - x_V = 19.03$ m. The corresponding Reynolds number $Re_{\chi,E} = \rho U_\infty \chi_E / \mu = 5.036 \times 10^7$, and the skin-friction coefficient, from equation (18.119), $c_{f,T}/2 = 0.0288 Re_{\chi,E}^{-0.2}$, is $c_{f,T}/2 = 8.298 \times 10^{-4}$. The shear stress at the end of the plate is then $\tau_{S,E} = \rho U_\infty^2 c_{f,T}/2 = 1.599$ Pa.

The drag force over the turbulent section D_T is obtained from

$$\begin{aligned} D_T &= W \int_{\chi_C}^{\chi_E} \tau_{S,T} dx = \mu U_\infty W \int_{Re_{\chi,C}}^{Re_{\chi,E}} \frac{c_{f,T}}{2} dRe_\chi = 0.0288 \mu U_\infty W \int_{Re_{\chi,C}}^{Re_{\chi,E}} Re_\chi^{-0.2} dRe_\chi \\ &= 0.0360 \mu U_\infty W \left(Re_{\chi,E}^{0.8} - Re_{\chi,C}^{0.8} \right) = 185.9 \text{ N}. \end{aligned}$$

The overall drag force on the plate is then $D_E = D_C + D_T = 190.1$ N.

- (iii) If the boundary layer were laminar over the entire length of the plate, the Reynolds number Re_E would have the value 5.292×10^7 , and the drag force would be given by

$$\begin{aligned} D &= \mu U_\infty W \int_0^{Re_L} \frac{c_{f,L}}{2} dRe_x = 0.3321 \mu U_\infty W \int_0^{Re_L} Re_x^{-0.5} dRe_x \\ &= 0.6642 \mu U_\infty W Re_E^{0.5} = 17.59 \text{ N}. \end{aligned}$$

- (iv) If the boundary layer were turbulent over the entire length of the plate, the drag force would be given by

$$\begin{aligned} D &= \mu U_\infty W \int_0^{Re_L} \frac{c_{f,T}}{2} dRe_x = 0.0288 \mu U_\infty W \int_0^{Re_L} Re_x^{-0.2} dRe_x \\ &= 0.036 \mu U_\infty W Re_E^{0.8} = 197.8 \text{ N}. \end{aligned}$$

Comments:

- At the transition location x_C we see that the shear stress for the laminar boundary layer is 0.369 Pa, whereas for the turbulent boundary layer the value is 4.14 Pa, i.e. an increase by an order of magnitude. These values should be regarded as indicative rather than 100% accurate, but it is clearly the case that the shear stress in a turbulent boundary layer is far in excess of that for a laminar boundary layer.
- Assuming the boundary layer to be turbulent over the entire plate would lead to an error in the overall drag of only +4%. In general, if the drag calculated assuming the flow is entirely turbulent is an order of magnitude (or more) greater than the drag due to laminar flow up to the transition location, then neglect of the laminar-flow contribution is justified.

18.14 Boundary layers with streamwise pressure gradient

In Section 18.13, concerned with the flat-plate boundary layer, it was found that an explicit relationship between c_f and Re_x resulted from the assumption of a power-law form for the velocity profile. The approach effectively neglects the outer-region wake contribution to the velocity profile, i.e. the wake parameter $\Pi = 0$, a simplification which cannot be justified where there is a streamwise pressure gradient, particularly an adverse gradient. Furthermore, in the latter case experiments show that Π can reach values as high as 100. Under such circumstances it is clear that the variation of $\Pi(x)$ has to be accounted for.

It is reasonable to assume that the momentum-integral equation (18.103) is still valid

$$\frac{c_f}{2} = \frac{d\theta}{dx} + (H+2) \frac{\theta}{U_\infty} \frac{dU_\infty}{dx} \quad (18.103)$$

where the normal-Reynolds-stress term has been neglected as before.

Equation (18.105) is also still valid

$$\frac{U_\infty \theta}{\nu} = Re_\theta = \left[\Pi + 1 - F(\Pi) \frac{1}{\kappa} \sqrt{\frac{c_f}{2}} \right] \frac{e^{\kappa \sqrt{2/c_f}}}{\kappa} e^{-(B\kappa + 2\Pi)}. \quad (18.105)$$

We also found earlier that the shape factor H corresponding to the combined log law plus law-of-the wake velocity distribution is given by

$$\frac{1}{H} = \frac{\theta}{\delta^*} = 1 - \frac{F(\Pi)}{(1 + \Pi)\kappa} \sqrt{\frac{c_f}{2}}. \quad (18.70)$$

Equations (18.105) and (18.70) can, in principle, be substituted into equation (18.103), leading to an equation involving dc_f/dx , $d\Pi/dx$, c_f , and Π , as well as the known (specified) quantities ν , κ , U_∞ , and dU_∞/dx . However, to proceed further requires additional information which cannot be obtained by manipulating any of the existing equations or derived from the Navier-Stokes equations. Various empirical equations have been proposed to provide this information, including an empirical **entrainment function**, in which the rate of entrainment into the boundary layer is related to the wake strength. Another approach is based upon an integral equation for kinetic-energy dissipation. With these empirical equations, solutions can be obtained using numerical integration. Such empirical approaches have now been superseded by much more sophisticated, and general, methods based upon the partial differential equations for the transport of turbulent kinetic energy, the rate of dissipation of turbulent kinetic energy, etc.

Qualitatively the influence of an adverse pressure gradient is similar to that for a laminar boundary layer, as discussed in Chapter 17, i.e. decreasing surface shear stress and, if the pressure-gradient parameter is sufficiently strong, boundary-layer separation. If the pressure gradient is favourable, there is a tendency for the turbulence intensity to reduce and ultimately to approach a laminar-like state, a process termed **laminarisation**, or **relaminarisation**.

18.15 Bluff-body drag

The force exerted by a flowing fluid on an immersed object is known as the **drag force**, or just **drag**. That part of the drag force due entirely to the surface shear stress acting on the object is called the **skin-friction drag**, or just **friction drag**. For a thin flat plate aligned with the flow, the drag is due entirely to friction drag. **Pressure drag**, or **form drag**, is the net force arising from the static pressure acting on an object's surface. For a thin flat plate normal to the flow, the drag is due entirely to pressure drag. For any object the sum of the form drag and the friction drag is called the **profile drag**. Additional contributions to profile drag come from **wave drag**, which in the case of marine craft arises from surface waves and in compressible flow from shockwaves, and the drag associated with lift known as **induced drag**.

Solid objects can be categorised as **streamlined** or **bluff** depending upon whether their shape is such that the flow over them remains attached, with accompanying low drag, or separates, with associated high drag. The flow over **low-drag aerofoils**, for example, may remain laminar but for most bodies of engineering interest the boundary layers will be turbulent over much of the surface as will be the region of flow downstream known as the **wake**. Although computer software has been developed which allows full details of the flow over complex shapes to be calculated quite accurately, for many engineering purposes it is sufficient to characterise the overall drag force D exerted on a body through a drag coefficient C_D defined by

$$C_D = \frac{D}{\frac{1}{2}\rho V^2 A} \quad (18.123)$$

where ρ is the fluid density, V is the flow velocity upstream of the body, and A is an appropriate area, usually the frontal projected (or silhouette) area of the body. It is to be expected that for any given shape, C_D will depend on the Reynolds number Re defined by

$$Re = \frac{\rho VL}{\mu}, \quad (18.124)$$

the Mach number M ,

$$M = \frac{V}{c}, \quad (18.125)$$

surface roughness, etc. In these equations μ is the dynamic viscosity of the fluid, c is the sound-speed, and L is a characteristic length of the body. For the most part we shall restrict attention to incompressible flow, which corresponds with M less than about 0.5.

The variation of C_D with Re for a long, smooth-surface, circular cylinder in crossflow is shown in Figure 18.7. The curve shown is based upon a number of experimental investigations carried out in the early-to-mid 20th century. The early data are included in the paper by Roshko (1961), who extended the range of conditions covered to $Re \approx 10^7$. The original experimental data exhibits considerable scatter, particularly for $Re > 4 \times 10^5$. Several flow regimes have been identified, some of which are evident from the C_D versus Re curve.

The flow at very low Reynolds numbers is initially steady, symmetric, and laminar without separation but as $Re \rightarrow 4$ a closed separation bubble appears attached to the downstream face of the cylinder. The vortices within the bubble grow, become unstable, are eventually ($Re > 50$) shed from alternate sides of the cylinder, and are advected downstream. The pattern of vortices

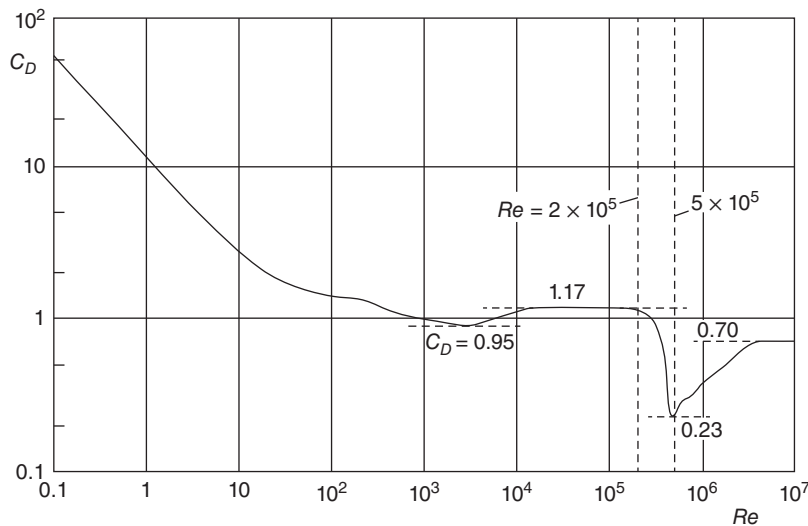


Figure 18.7 Drag coefficient C_D versus Reynolds number Re for a smooth circular cylinder in crossflow (logarithmic scales)

of alternating rotation is known as a **Kármán vortex street**. The frequency f corresponding to successive vortices passing a fixed point satisfies the equation

$$St = \frac{fD}{V} \approx 0.2 \quad (18.126)$$

for $40 < Re < 60 - 100$. The vortices are stable until $200 < Re < 400$, when they become unstable. The drag coefficient decreases progressively with increasing Re , reaching a first minimum of $C_D \approx 0.95$ at $Re \approx 2000$.

Once $Re > 400$ the vortices are already turbulent as they detach from the cylinder although the boundary layer on the cylinder surface remains laminar until $Re \approx 2 \times 10^5$ with separation occurring slightly before 90° measured from the forward stagnation line. A wide turbulent wake is created downstream of the cylinder, within which the static pressure is much lower than the free-stream pressure. From the minimum at $Re \approx 2000$ the drag coefficient increases slightly until $Re \approx 10^4$ and then remains constant at about 1.2 until $Re \approx 2 \times 10^5$. At this Reynolds number the boundary layer on the cylinder transitions from laminar to turbulent and remains attached until about 120° from the stagnation line. The turbulent wake is now narrower than before, the static pressure is close to its free-stream value, and the drag coefficient much lower with a minimum value $C_D \approx 0.23$ at $Re \approx 5 \times 10^5$. The sudden drop in C_D at $Re \approx 2 \times 10^5$ is referred to as the **drag crisis**, and the corresponding value of Re as the **critical Reynolds number**, Re_C . If $Re < Re_C$ the flow is said to be **subcritical**, and **supercritical**¹⁸⁷ if $Re > Re_C$. Beyond this point the drag coefficient increases progressively until it appears to plateau at a value of 0.7 at $Re \approx 4 \times 10^6$. Although there are no data for $Re > 10^7$, from a practical point of view this is unlikely to cause problems: for a 50 mm-diameter cylinder with flow of air at 50°C the velocity corresponding with $Re = 10^7$ would be 3000 m/s (i.e. for air at STP a Mach number close to 9, and for a 1 m diameter cylinder it would be 150 m/s ($M = 0.44$)).

The variation of C_D with Re for a smooth sphere is qualitatively similar to that for a circular cylinder although the plateau value in the range $10^3 < Re < 2 \times 10^5$ is much lower at about 0.4. The critical Reynolds number for a sphere or cylinder is reduced significantly by surface roughness, trip wires, and free-stream turbulence. For example, at $Re \approx 10^5$ the drag coefficient for a dimpled golf ball is less than 50% of the value for a smooth sphere.

Once the Mach number exceeds about 0.4 compressibility effects become important and C_D begins to increase, initially gradually but dramatically so in the vicinity of $M = 1$ as shockwaves arise.

Drag coefficients reported in the literature for long cylinders of various cross section in crossflow are given in Figure 18.8, and for various three-dimensional objects in Figure 18.9. In all cases the approach flow is from left to right. It is a great simplification to present C_D values as a single number but, as we have seen for a smooth circular cylinder, C_D is approximately constant in the range $10^4 < Re < 2 \times 10^5$, and the same is true for a similar Re range for most of the shapes in these two figures. The values listed are an average from several sources, some of which for a given object differ by as much as 20%. In these two figures, each object is considered in isolation, whereas in practice it is often the case that there are two or more

¹⁸⁷ The terms 'subcritical' and 'supercritical' as used here should not be confused with the same terms used for open-channel flow.










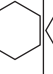



square		R/H	0	0.02	0.17	0.33			
		C_D	2.15	2.0	1.2	1.0			
square		C_D	1.6						
rectangle		L/H	≤ 0.4	0.4	0.5	0.65	1.0	1.2	2.0
		C_D	1.9	2.4	2.4	2.9	2.2	2.1	1.7
rectangle with rounded nose $R/H = 1$		L/H	0.5	1.0	2.0	4.0	6.0		
		C_D	1.15	0.90	0.70	0.68	0.64		
rectangle with rounded nose and taper		C_D	0.15						
semi circle		C_D	1.9						
semi-circular shell		C_D	2.3						
semi-circular shell		C_D	1.1						
ellipse		L/H	1.0	2.0	4.0	8.0			
		C_D	0.3	0.2	0.15	0.1			
hexagon		C_D	1.0						
hexagon		C_D	0.7						
equilateral triangle		R/H	0	0.02	0.08	0.25			
		C_D	1.5	1.2	1.3	1.1			
equilateral triangle		R/H	0	0.02	0.08	0.25			
		C_D	2.15	2.0	1.9	1.3			

Figure 18.8 Typical drag coefficients for long cylinders in crossflow




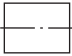





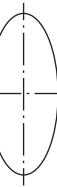
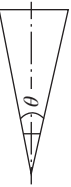

cube		C_D	1.06																
cube		C_D	0.81																
rectangular plate normal to flow		B/H	1	5	10	20	∞												
		C_D	1.18	1.2	1.3	1.5	2.0												
circular cylinder normal to flow		H/D	1	2	3	5	10												∞
		C_D	0.64	0.68	0.74	0.74	0.82												1.2
circular cylinder aligned with flow		L/D	$\ll 1$	0.5	1	2	4												
		C_D	1.16	1.13	0.92	0.84	0.86												
solid hemisphere		C_D	1.17																
solid hemisphere		C_D	0.42																
hollow hemisphere		C_D	1.41																
hollow hemisphere		C_D	0.39																
ellipsoid		L/D	0.75	1	2	4	8												
		C_D	0.2	0.2	0.13	0.1	0.08												
cone		θ	10°	20°	30°	40°	60°												
		C_D	0.3	0.4	0.55	0.65	0.8												
streamlined body		C_D	0.04																

Figure 18.9 Typical drag coefficients for various three-dimensional objects

objects in close proximity. The situation is then more complex and it is not realistic to list all the possible shape combinations.

In Figure 18.8 the streamwise length of each cylinder is L , its height is H , and, where the corners of an object have been rounded, R denotes the corner radius. The projected area A is given by BH , where $B (\gg H)$ is the cylinder span.

The benefit of rounding corners is clearly evident from the entries for square and triangular cross sections. Even more striking is the drag reduction associated with rounding to $R = 0.5 H$ the nose of a cylinder of rectangular cross section. Tapering the base of a rectangular cross section with such a rounded nose reduces the drag coefficient to 0.15, the level for an elliptical cross section with aspect ratio 4:1.

In Figure 18.9, for the cube, H is the side length; for the rectangular plate, H is the height, and B is the span; for the axisymmetric three-dimensional objects, D is the maximum diameter; for the cylindrical cylinder aligned with the flow, L is the length; for the cylindrical cylinder normal to the flow, L is the height; and for the cone, θ is the total included angle. The corresponding projected areas A are H^2 , $\sqrt{2}H^2$, BH , HD , and $\pi D^2/4$.



18.16 SUMMARY

In this chapter we have outlined the principal characteristics of a turbulent flow and shown how Reynolds time-averaging procedure, applied to the Navier-Stokes equations, leads to a set of equations similar to those governing laminar flow but including additional terms which arise from correlations between fluctuating velocity components and velocity-pressure correlations. We showed that dimensional considerations applied to the kinematic viscosity, and the rate of dissipation ϵ of specific turbulent kinetic energy k leads to the Kolmogorov time, length, and velocity scales which characterise the smallest eddies of turbulent motion. The complex nature of turbulent motion has led to an empirical methodology called turbulence modelling in which the correlation terms in the Reynolds-averaged Navier-Stokes equations and in the transport equations for k , ϵ , and other turbulence quantities are modelled. We show that limited, but useful, results for fully-developed turbulent channel flow and zero-pressure-gradient boundary layers can be deduced by treating the turbulent shear flow in the immediate vicinity of a solid surface as a Couette flow which leads to the Law of the Wall and the logarithmic velocity variation termed the log law. We discuss the characterisation of surface roughness, and its effect on both the velocity distribution and surface shear stress. It is shown that the distribution of mean velocity within a turbulent boundary layer can be represented by a linear combination of the near-wall log law and an outer-layer Law of the Wake.

The student should be able to

- give a qualitative description of turbulent flow
- understand Reynolds' decomposition and the derivation of the Reynolds-averaged Navier-Stokes equations
- use dimensional analysis to derive the Kolmogorov length, time, and velocity scales
- explain why turbulence modelling is necessary
- use dimensional analysis to show that the velocity distribution in the near-wall region of a turbulent shear flow has the universal form $u^+ = f(y^+)$
- show that within the viscous sublayer $u^+ = y^+$
- show that if viscosity has no direct influence on the velocity distribution then $u^+ = \ln y^+/\kappa + B$

- understand the qualitative behaviour of a boundary-layer velocity profile described by the combination of the log law and the law of the wake and the role of the wake parameter Π
- derive an equation for the dependence of the Fanning friction factor on the Reynolds number for fully-developed turbulent flow through a pipe assuming that the velocity distribution follows the log law
- apply the individual loss coefficients for various pipe fittings to calculate the pressure loss through a piping system
- understand the influence of surface roughness on the near-wall velocity distribution in a turbulent flow
- derive an equation for the dependence of the skin-friction coefficient on the momentum-thickness Reynolds number Re_θ for a flat-plate turbulent boundary layer, assuming that the velocity distribution follows the log law plus Law of the Wake combination
- derive an equation for the dependence of the skin-friction coefficient on the streamwise Reynolds number Re_x for a flat-plate turbulent boundary layer, assuming that the velocity distribution follows the log law plus Law of the Wake combination
- derive an equation for the dependence of the skin-friction coefficient on the momentum-thickness Reynolds number Re_θ for a flat-plate turbulent boundary layer, assuming that the velocity distribution has a power-law form
- derive an equation for the dependence of the skin-friction coefficient on the streamwise Reynolds number Re_x for a flat-plate turbulent boundary layer, assuming that the velocity distribution has a power-law form
- make use of drag coefficients to calculate the drag force acting on an object of given shape



18.17 SELF-ASSESSMENT PROBLEMS

- 18.1** Show that, for an incompressible flow,

$$u \frac{\partial u}{\partial x} + v \frac{\partial u}{\partial y} + w \frac{\partial u}{\partial z} = \frac{\partial u^2}{\partial x} + \frac{\partial (uv)}{\partial y} + \frac{\partial (uw)}{\partial z}$$

where the symbols have their usual meaning.

- 18.2** Show that, for fully-developed turbulent flow through a smooth-wall circular pipe, neglect of the contribution of the viscous sublayer to the mean-velocity distribution is valid if

$$\sqrt{\frac{2}{f_F}} \frac{1}{Re_D} \ll 1$$

where $f_F = 2\tau_S/\rho \bar{V}^2$ is the Fanning friction factor, $Re_D = \rho \bar{V} D/\mu$ is the pipe Reynolds number, τ_S is the surface shear stress, \bar{V} is the bulk-mean velocity, D is the pipe diameter, ρ is the fluid density, and μ is the dynamic viscosity of the fluid.

- 18.3** Water at 10 °C is pumped through a pipeline which consists of a 50 mm diameter pipe 25 m long followed by an 80 mm diameter pipe also 25 m long. The relative roughness for both pipes is 0.001. The two sections of pipe are connected by a sharp-edged sudden expansion. Entry to the 50 mm pipe and exit from the 80 mm pipe

are both sudden with sharp edges. A threaded 90° standard elbow is installed in the 50 mm pipe, and a threaded 90° long-radius elbow in the 80 mm pipe. The flow is controlled by a valve in the 80 mm pipe, for which the loss coefficient is 6.0 when the valve is fully open. If the flowrate is 0.011 m³/s calculate the overall loss in stagnation pressure and the pumping power required to maintain the flow. (Answers: 0.235 MPa, 2.583 kW)

- 18.4** Assume that for fully-developed turbulent flow through a rough-wall circular pipe the velocity distribution is given by the equation

$$u^+ = \frac{1}{\kappa} \ln y^+ + B - \frac{1}{\kappa} \ln (1 + 0.3\epsilon^+).$$

Show that the bulk-mean velocity \bar{V} for a pipe of diameter D is given by

$$\bar{V}^+ = \frac{1}{\kappa} \ln \left(\frac{R^+}{1 + 0.3\epsilon^+} \right) + B - \frac{3}{2\kappa}$$

and hence that the Fanning friction factor f_F is related to the Reynolds number Re_D and the relative roughness ϵ/D through the formula

$$\sqrt{\frac{2}{f_F}} = \frac{1}{\kappa} \ln \left[\frac{\sqrt{\frac{f_F}{2}} Re_D}{2 \left(1 + 0.3 \frac{\epsilon}{D} \sqrt{\frac{f_F}{2}} \right)} \right] + B - \frac{3}{2\kappa}.$$

- 18.5** Show that, for a boundary layer with $\Pi = 0$, the streamwise variation of the skin-friction coefficient is given by

$$Re_x = \frac{1}{\kappa^3} (\beta^2 - 4\beta + 6) e^{(\beta - B\kappa)}$$

where $\beta = \kappa \sqrt{2/f_F}$.

If $\kappa = 0.4$, $B = 5.5$, and $c_f/2 = 7.15 \times 10^{-4}$, find the value of Re_x using this formula. Use the calculated value of Re_x to calculate $c_f/2$ from White's formula:

$$\frac{c_f}{2} = \frac{0.2275}{\ln^2 (0.06 Re_x)}.$$

(Answer: 1.531×10^9 , 6.767×10^{-4})

Comments:

The two values of $c_f/2$ are within about 5.5% of each other.

Note that with $\Pi = 0$ it has been assumed that the log law applies throughout the boundary layer. This is exactly the same assumption made in the analysis of fully-developed turbulent pipe flow. The key difference here is that the boundary-layer thickness increases with streamwise distance whereas the pipe diameter is fixed.

- 18.6** Assume that for fully-developed turbulent flow through a parallel-wall channel of height $2H$ the velocity distribution is given by the log law

$$u^+ = \frac{1}{\kappa} \ln y^+ + B.$$

Show that the bulk-mean velocity \bar{V} is given by

$$V^+ = \frac{1}{\kappa} \ln H^+ + B - \frac{1}{\kappa}$$

and hence that the Fanning friction factor f_F is related to the Reynolds number $Re_H = 2\bar{V}H/\nu$ through the formula

$$\sqrt{\frac{2}{f_F}} = \frac{1}{\kappa} \ln \left(\frac{1}{2} \sqrt{\frac{f_F}{2}} Re_H \right) + B - \frac{1}{\kappa}.$$

18.7 Use the power-law equations

$$\frac{c_f}{2} = 0.0288 Re_x^{-0.2}$$

and

$$\frac{c_f}{2} = 0.0225 Re_\delta^{-0.25}$$

to calculate the skin-friction coefficient $c_F/2$, the wall shear stress τ_S , the friction velocity u_τ , and the boundary-layer thickness δ at the end of a flat plate 20 m long if the free-stream velocity is 70 m/s and the flowing fluid is air at 25 °C. Assume the boundary layer is turbulent starting at the leading edge of the plate.

Calculate the Kolmogorov scales given by

$$l_K = \left(\frac{\nu^3}{\epsilon} \right)^{1/4}, \quad \nu_K = (\nu\epsilon)^{1/4}, \quad \text{and} \quad \tau_K = \left(\frac{\nu}{\epsilon} \right)^{1/2}$$

and the turbulent-energy dissipation rate given by

$$\epsilon = \frac{u_\tau^3}{\kappa y},$$

where the von Kármán constant $\kappa = 0.41$, at a distance 1 mm from the plate surface.

Calculate the ratios l_K/δ , ν_K/U_∞ , and $\tau_K U_\infty/\delta$.

(Answers: 7.395×10^{-4} ; 4.290 Pa; 1.904 m/s; 191.3 mm; 21.82 μm ; 0.725 m/s; 30.1 μs ; $1.682 \times 10^4 \text{ m}^3/\text{s}^2$; 1.184×10^{-4} ; 0.014; 0.0110)

18.8 Write the log law for a boundary layer in terms of u/U_∞ , $U_\infty y/\nu$, $c_f/2$, and the log-law constants B and κ . Suggest how a value for the friction factor could be obtained from an experimentally determined velocity distribution, $u(y)$.

18.9 Show that the following form of the Kármán-Nikuradse formula for turbulent flow through a smooth pipe,

$$\frac{1}{\sqrt{f_D}} = -2 \log_{10} \left(\frac{2.51}{Re_D \sqrt{f_D}} \right)$$

can be transformed into the form

$$\sqrt{\frac{2}{f_F}} = 2.457 \ln \left(\sqrt{\frac{f_F}{2}} Re_D \right) + 0.292$$

where $f_F = \tau_S/\rho \bar{V}^2$ is the Fanning friction factor, $f_D = 4f_F$ is the Darcy friction factor, and $Re_D = \rho \bar{V}D/\mu$ is the Reynolds number.